Novel Low Dielectric Constant Thin Film Materials by Chemical Vapor Deposition

Viktor Simkovic

Thesis submitted to the Faculty of the
Virginia Polytechnic Institute and State University
In partial fulfillment of the requirements for the degree of

Master of Science
In
Materials Science and Engineering

Dr. Robert Hendricks, chair
Dr. Seshu B. Desu
Dr. William Reynolds
Dr. Willi Graupner

July 16, 1999
Blacksburg, Virginia

Keywords: Chemical Vapor Deposition, Low-k, Thin Films, Dielectric Constant, Parylenes

Novel Low Dielectric Constant Thin Film Materials by Chemical Vapor Deposition

Viktor Simkovic

(ABSTRACT)

A modified CVD reactor was designed with a deposition chamber capable of accomodating 8" wafers, with the capacity to remotely pyrolyze two different precursors. The design was based on a previous working reactor, with the most notable improvements being a showerhead design for more even delivery of gaseous precursor and a separate heating control of the substrate holder and deposition chamber walls. The performance of the reactor was analyzed by testing the pressure gradients within and the thickness uniformity of films deposited on 8" wafers. The reactor exhibited a linear pressure gradient within, and the thickness uniformity was excellent, with a slight increase in thickness towards inlet of the showerhead. The thickness difference between the maximum and minimum thickness on an 8" wafer was 14%. Films of polyparaxylylene (PPXN), polychloroparaxylylene (PPXC), SiO_2, and PPXC/SiO_2 were deposited, with deposition rates and indices of refraction comparable to those obtained on the old reactor design. A full factorial study was performed to determine the effect of the substrate temperature, the sublimation temperature, and the pyrolysis temperature on the deposition rates of PPXC. It was determined that the substrate temperature has the greatest effect, with about 50% contribution, and deposition rates increased with decreasing substrate temperature. The sublimation temperature contributed 25%, with increasing sublimation rates leading to higher deposition rates. The pyrolysis contributes very little, with about 2%, and the variance ratio did not fall within a 90% confidence level.

A low dielectric constant polymer, poly(tetrafluoro-*p*-xylylene) (VT-4), was synthesized by chemical vapor deposition from 4,5,7,8,12,13,15,16-octafluoro-[2.2]-paracyclophane (DVT-4). The main motivation was to find a cheaper alternative to poly(alpha, alpha , alpha ', alpha '-tetrafluoro-p-xylylene) (AF-4) with similar properties. The dielectric constant of VT-4 was measured as 2.42 at 1 MHz, and the in-plane and out-of-plane

indices of refraction were 1.61 and 1.47 at 630 nm. The large negative birefringence suggests a low out-of-plane dielectric constant, which is desired for interlayer dielectrics. The VT-4 polymer was found to be stable at 460 $^{\circ}$C by thermogravimetric analysis (TGA).

Polymer/Siloxane nanocomposites were studied as an alternate path to a polymer/silica composite. This study showed that incorporation of a four-ringed liquid siloxane precursor into the parylene PPXC is not feasible. A solid precursor cube-like molecule, vinyl-T8, was incorporated with ease. Pyrolysis of vinyl-T8 at different temperatures revealed complex behavior, with the formation of polymerized vinyl-T8 (through free radical addition at the vinyl groups) as well as silica-like structures forming above 500 $^{\circ}$C as a result of the breaking up of the cage structure of vinyl-T8. Codepositions of PPXC and vinyl-T8 were then examined as a possible path towards a polymer/silica nanocomposite. At deposition temperatures below 5° C, precipitation of excess vinyl-T8 into cubic micron-sized crystals occurred. As this was undesirable, studies were continued at higher deposition temperatures. A Taguchi orthogonal array was set up to study the effect of the sublimation temperatures of the two precursors as well as the pyrolysis temperature and the substrate temperature on the deposition rate, the index of refraction and the weight loss after a 500 $^{\circ}$C anneal. The deposition rate depended mostly on the sublimation temperature of the PPXC and the substrate temperature. The lowest index of refraction (and thus the lowest dielectric constant) was obtained with the lowest sublimation temperatures of 134 $^{\circ}$C for PPXC and 195° C for vinyl-T8 and a pyrolysis temperature of 200 $^{\circ}$C. Each of the factors was found to have an effect on the index of refraction, with the sublimation temperature of vinyl-T8 having the most influence. The films degraded at 500 $^{\circ}$C, indicating that post-deposition annealing of the films did not lead to a conversion of the vinyl-T8 to a SiO_2-like structure (which would be stable at that temperature). X-ray diffraction spectra of the films revealed peaks which were not present for any of the vinyl-T8 films or characteristic of PPXC. Therefore, some type of interaction between the two components occurred and affected the morphology, most likely the formation of a block copolymer. Thus, though polymer/silica films were not attained, the resulting composites had comparable properties with higher deposition rates and a cleaner process.

ACKNOWLEDGEMENTS

TABLE OF CONTENTS

Introduction

Chapter 1 - *Scale-Up Study of a Modified CVD Reactor*

Chapter 2 - *VT-4: A New Low-k Polymer*

Chapter 3 - *Polymer/Siloxane Nanocomposites*

Chapter 4 - *Summary and Future Work*

Motivation

Progress is driven by improvements, which are measured by either a more efficient functionality of a technological product or the process of its manufacture. In the semiconductor industry, better performance is marked by higher device speed as well as an increase in the packing density. This increase in density leads to higher circuit complexity, requiring a greater number of interconnects, leading to smaller wire width and spacing. As these dimensions approach the transistor gate length, in the 0.25 μm regime, the speed of the IC is no longer dominated by the switching speed of the transistor. Rather, the interconnect delay caused by RC coupling becomes significant. As the feature size decreases, the interconnect delay comes to be the major part of the total delay.[1]

This time delay depends on the resistance of the interconnects and the capacitance between them. The capacitance depends on the metal pitch, which is the sum of the metal width and the spacing in between, the metal thickness and length, and the dielectric constant of the space in between the metal. The RC delay is the product of this resistance and capacitance. The main strategies for reducing the delay are increasing the number of metallization levels, replacing the aluminum interconnects with a better conducting metal like copper, or replacing the interlayer dielectric, currently SiO_2, with a material with a lower dielectric constant, k. SiO_2 has a k of 3.9-4.0, and the new candidate will have a k anywhere from 3 to the lowest attainable value, which is 1, the dielectric constant of air. Several classes of materials qualify, most of them polymers or inorganic polymers. The dielectric constant of polymers ranges from 3.5 down to the k of polytetrafluoroethylene, which is 2.06. Other options include nanocomposites or porous materials, such as nanoporous silica.[2]

Other properties of the new interlayer dielectric (ILD) of importance are the dielectric loss, the breakdown voltage, the thermal stability, thermomechanical characteristics, good adhesion and gap filling ability, low moisture uptake, high thermal conductivity, low leakage current, and finally, low cost. Of the highest significance is the thermal stability, for the processing conditions call for temperatures of 400 ^{o}C to 450 ^{o}C. Since

1

most alliphatic bonds in polymers breakdown around 400 ^{o}C, this puts a definite constraint on the type of polymer that is suitable as a new ILD. The incorporation of a new material entails the modification of both the process as well as the architecture of the IC. Two main deposition techniques for low-k materials are spin coating and chemical vapor deposition (CVD). While spin coating lends itself to a much wider class of materials and deposition conditions are easier to establish and control, the current process employs CVD, thus this is the processing technique of preference.[3]

The equipment required for CVD is intricate and optimization of the deposition conditions and film quality involves many parameters. Therefore, improvements in material properties entail improvements in the process, which in turn calls for continuous upgrading of equipment. The purpose of this work is to describe, justify and confirm design improvements in a CVD reactor system over a pre-existing design, and then to present two studies of novel low-k materials that aim to satisfy the current demand for a new ILD.

Literature Review

Chapter 1

The two main techniques for depositing thin films in wide use today are physical vapor deposition, the category under which methods such as evaporation and sputtering fall, and chemical vapor deposition (CVD). CVD offers many advantages most important of which are low cost and excellent step coverage and uniformity, and has thus become the dominant technique in industry.

The first CVD techniques were employed in the late 1880's to coat thin metallic films onto incandescent filaments.[4-6] The formation of high purity metallic thin films made by chemical transport first received interest at about the same time period, but progress in the CVD field progressed little until the 1930's, when deposition of refractory compounds gained technological importance.[7] With the development of solid state electronics in the 1950's, carbon coating of graphite susceptors used in the zone-refining process of germanium was accomplished with chemical vapor deposition. In 1960, the replacement of Ge with Si as the main semiconducting material and the development of the planar technology by Hoerni caused a rapid expansion of interest in CVD technology.[8] Homoepitaxial films of silicon achieved device quality and became used for the manufacture of all types of semiconducting devices. Compounds such as GaAs and heterojunctions were also first obtained at the same time. Further research into chemical vapor deposition processes led to the development of polycrystalline semiconducting films as well as doped amorphous semiconductors, important for the optoelectronics field.

Due to technological driving forces, most of the emphasis has been on the evolution of deposition techniques leading to better film quality, less so on the understanding of the basic sciences behind the processes such as thermodynamics, kinetics, or growth and nucleation. Originally, films were prepared at atmospheric pressure and high temperatures. Deposition temperatures below 500 $^{\circ}$C were first employed by Goldsmith and Kern in 1967 to obtain SiO_2.[9] Organometallic chemical vapor deposition (MOCVD),

which uses organic molecules to deliver metallic elements to the substrate, was first utilized by Manasevit in 1968.[10] Low pressure chemical vapor deposition (LPCVD) was first demonstrated by Sandor (1962) and Kern (1965) for the deposition of SiO_2.[11,12] Another technique of significance is plasma enhanced CVD (PECVD), which uses plasma instead of thermal activation to impart the necessary energy for the reaction to occur and was first reported in 1965 by Sterling and Swan for the deposition of amorphous silicon, SiO_2, and Si_3N_4.[13]

The first types of reactors were RF heated vertical, horizontal, and pancake cold-wall reactors.[14,15] Later improvements included the rotary disc reactor which is used for batch processing, the radiant-heated barrel reactor, and the RF-heated barrel reactor.[16-18] Continuous processing reactors, using either laminar flow nozzles for gas dispersion or a slotted dispersion plate, were introduced in 1975 by Pacific Western System, Inc. For laboratory experimentation and research, the single wafer vertical or horizontal resistance-heated reactor is used most often.

Thermodynamical analysis of CVD processes was first undertaken by Arizumi, Ban, Sirtl, as well as Eriksson, Spear, Shaw, and Bernard in the 1970s.[19-20] The kinetics of gaseous flow and deposition in CVD reactors were first studied by Shaw (1974).[21] The understanding of the behavior and flow of gaseous species within a reactor was greatly ameliorated by the development of methods such as gas chromatography, mass spectroscopy, absorption spectroscopy, and Raman spectroscopy, which allowed in-situ detection of gaseous species. Transport phenomena, important in the optimization of flow within a reactor, were first studied in the 1970's by Everteijn, Berkman, Takahashi, and Ban.[22] Models which combined fluid mechanics and chemical kinetics begun to appear in the 1980s. Most models focused on the decomposition and deposition of silicon from silane, as this remains the most significant CVD process for the semiconductor industry.[23-24] The development of the stagnation point flow reactor, which obviated the need for a rotating substrate by developing a uniform boundary layer adjacent to the substrate led to improved uniformity and reproducibility over multiwafer batch processes.[25-28] In a stagnation point reactor, a gas distributor such as a porous

medium creates uniform gas flow perpendicular to the substrate, creating a vertically impinging jet leading to a uniform boundary layer above the substrate. The nature of the gas distributor, the pressure drop across the distributor, the deposition chamber inlet shape and dimensions, and the extent of thermal convection are the main factors in the performance of this kind of reactor.[26]

Desu and Kalidindi addressed the problem of determining the rate controlling step in a CVD process from deposition rate profiles. A regime can be either gas-phase controlled and surface controlled, and knowing which regime is dominant is essential for optimization.[29]

This work describes the design and performance analysis of a horizontal CVD reactor with a showerhead design, which approaches a stagnation point design. The reactor described is a scaled-up version of a previous design, which has been used successfully to obtain films for low-k research such as polymers from the parylene family, low temperature thermal SiO_2, and polymer/SiO_2 nanocomposites.[30-32]

Chapter 2

The class of polymers known as parylenes is well studied. Szwarc was the first one to report the chemical vapor polymerization of poly-para-xylylene (PPXN) from a xylene monomer precursor in 1947.[33] The yields from this reaction were only 10-15% at a pyrolysis temperature of 900-950 ^{o}C, and 25% at 1150 ^{o}C. Though some researchers like Kaufman and Corlely studied the properties of PPXN, the low yields and high temperatures required discouraged further interest.[34,35]

In 1966, Gorham discovered that PPXN could be obtained from dicyclo-*p*-xylylene, a dimer, at temperatures of 600 ^{o}C with very high yields.[36] The Gorham process, whose reaction pathway is shown in Figure 1, furthermore eliminated the undesirable side reaction, cross-linking, and oligomerization which occurred at the higher
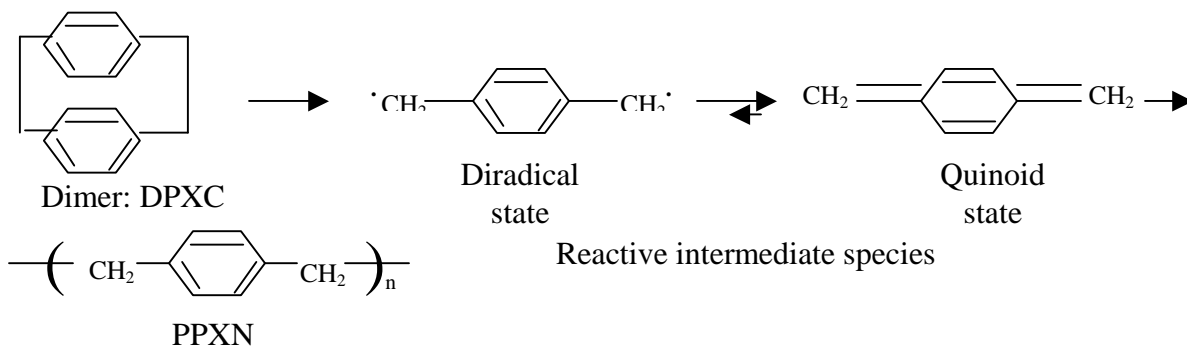
Figure 1 – The Gorham Process

reaction temperatures. The chemistry of the process has been well described. The pyrolysis of the dimer leads to a reactive species which oscillates between a diradical and a quinoid state, spending most of the time in the more stable quinoid state. For polymerization to occur, monomers in the high energy diradical state have to react on the substrate and initiate the reaction. Thus the polymerization is self-initiating and the order of the initiated species was determined to be three.[37-43] The reason polymerization does not occur in the gas phase is the fact that the required collision of three diradical species in the gas phase is very unlikely. Other dimer precursors have been employed to obtain parylenes with substituents on the benzene ring, most notable of which are poly-para-chloroxylylene and poly-para-dichloroxylylene.

The effect of deposition conditions such as the substrate temperature, the sublimation temperature, and pyrolysis temperature on the deposition rate and morphology of the films was determined by a number of researchers.[44-50] In 1978 Beach developed a quantitative model for deposition describing steady-state solutions in one dimension.[51] The model obtained equations relating the growth rate and molecular weight of the film to parameters such as the order of initiation, initiation and propagation rate constants, diffusion constant of the monomer in the film, and the vapor pressure of the monomer. While the model was consistent with the limited data available, there was some discrepancy between the observed and predicted growth rates. This discrepancy was eliminated by Gaynor and Desu, who extended the model to two dimensions, thus obtaining a better method of measuring the growth rate as a function of the monomer partial pressure.[52]

Characterization of the parylenes has been done to determine their morphology and phase transformations.[53-62] The films as deposited are semicrystalline, with crystallization following polymerization, yielding monoclinic crystals. PPXN undergoes an irreversible phase transformation at 220 ^{o}C to a hexagonal crystal structure. Optical properties have not been studied extensively until recently.[63]   Determination of the molecular weight of the polymers presents a problem since the films are nearly insoluble. However, since there is no termination reaction, each chain contains a free radical which is in time neutralized by water vapor or oxygen. If the film is analyzed right after deposition, electron paramagnetic resonance spectroscopy of the free radical end group or neutron activation analysis can be utilized to determine the molecular weight.[64,65] A dissertation by Gaynor studied the optical properties of parylenes and developed a method for the copolymerization of parylenes in which the parylene is used as an initiator to obtain a new CVD homopolymer.[66-69]

Several overviews of the progress made in the study of the parylenes have been published. Szwarc and Beach summarized much of the work that was done up to the 70's and 80's.[70,71] The applications of the parylene films are extensive. The polymers have been studied or utilized for such diverse uses as waterproof coatings, x-ray windows, passivation layers for biomaterials, dielectric in high performance capacitors, coatings for circuit boards, and of course as interlayer dielectrics.[72-77] As an interlayer dielectric, poly(aliphatic tetrafluoroparaxylylene) has received much interest recently, as it has the lowest dielectric constant of the parylenes.[78-81]

This work reports the synthesis and characterization of a new polymer in the parylenes class, polytetrafluoroxylylene, or VT-4. This polymer is well suited for low-k applications due to its low dielectric constant, high thermal stability, and low price and availability of the precursor.

Chapter 3

 Before any attempts were made to deposit organic-inorganic composites, a process to deposit an inorganic phase which was compatible with the parylene deposition process

had to be developed. Poly-*p*-xylylene (PPXN) has a ceiling deposition temperature of 30 $^{\circ}$C, while poly-chloro-*p*-xylylene (PPXC) has a ceiling deposition temperature of 90 $^{\circ}$C. Above these temperatures, deposition does not occur. Conventionally, SiO_2 is deposited at temperatures of 650 $^{\circ}$C with TEOS as the precursor, and 450 $^{\circ}$C with DADBS as the precursor. Such a method was developed by Senkevich and Desu, utilizing the pyrolysis of DADBS, achieving SiO_2 films at deposition temperatures of 70 $^{\circ}$C.[82] The next step undertaken was the deposition of polymer-silica multilayers. This was accomplished by simply alternately opening and closing the respective valves of the organic and inorganic precursors.[83] The resulting films shed some light into the properties of ultra-thin polymeric films, as it is observed that the films with thickness below 100 nm are severely constrained by the substrate.[84]

Several studies recently investigated organic/inorganic hybrids or composites. One group developed a hybrid consisting of a matrix of organically modified silicate with a phase-separated thermoplastic polymer embedded within the matrix. The motivation was for toughening brittle sol-gel condensates. The inorganic matrix was produced by hydrolysis of functionalized silsesquioxanes, and the polymers used were functionalized polyimides.[85] Such hybrid materials have been show to be stable to 400 $^{\circ}$C and form tough, crack-free films.[86] Inorganic-organic composites were also synthesized through the hydrolysis and condensation of diethoxymethylsilane and methyltriethoxysilane alkoxides for optical applications.[87] Xiaochun and King studied PMMA/gel silica glass composites with Raman and IR spectroscopic methods and found that the two phases interact through hydrogen bonding. These hybrids were found to be hydrophobic due to the elimination of adsorption sites present in typical sol-gel silica.[88] Another group used tetraethoxysilane and 2-hydroxybenzyl alcohol in a sol-gel reaction to obtain hybrids consisting of silica and phenolic resins.[89] For waveguide applications, polydimethylsiloxane and oxides of silicon, germanium, and titanium were combined in a sol-gel process.[90] Most of the research has thus focused on sol-gel techniques of making inorganic-organic composites.

Gaynor, Senkevich, and Desu developed a method of creating copolymer films by CVD by using the parylenes as an initiator. The method relies on a combination of comonomer and deposition temperature such that the PPXN obeys surface reaction control, while the comonomer is in the mass control regime. Under these conditions, the diradical PPXN reactant mostly reevaporates after condensing on the substrate, while the comonomer stays. The small amount of PPXN which adheres to the substrate acts as an initiator for the polymerization of the comonomer. With this technique, many comonomer can be combined with PPXN to form new CVD polymeric materials.[91] Gaynor extended this technique to copolymerizing inorganic comonomers with some success.[92]

Thermal CVD nanocomposites were recently developed using PPXC and SiO_2 as the two components which formed with no covalent bonding between the phases. The composition of the two phases is easily varied by controlling the vapor pressures of the two precursors.[93] However, the low temperature thermal CVD process of depositing silica by this method results in reactive species which deposit at any temperature. Thus the reaction is surface controlled and results in a rapidly descending deposition rate profile. This results in low deposition rates on the substrate as the reactive intermediate is rapidly depleted along the way. Furthermore, the deposition of silica along the gas pathway results in the formation of a rough surface with a large surface area, which increases with the number of depositions made. Eventually, no reactive species reaches the substrate, as it all reacts on the available surface before reaching the deposition chamber. Silica is very hard and adheres to metal surfaces very well, making cleaning the reactor a time consuming process. Thus a new source for the inorganic phase was investigated in this work, namely cyclic and polyhedral oligosilsesquioxanes.

Some work has been done studying hydridospherosiloxanes for dielectric applications. The molecules are cagelike sphere with Si atoms at the vertices bridged by oxygen atoms. HT8 and HT10, which have 8 and 10 Si atoms per molecule respectively, have been used as precursors to obtain SiO_2 films at deposition temperatures of 500 ^{o}C.[94,95] Polysilsesquioxanes deposited with spin-coating techniques have been analyzed and their dielectric properties reported.[96] It was found that the dielectric constant of these

materials is closer to 3, which is lower than pure silica, which has a k of 3.9-4.0. Finally, vinyl-T8, the precursor investigated in this work has been used to obtain dielectric films by subliming it and subsequently causing polymerization to occur by plasma treatment.[97]

REFERENCES

1. W.W. Lee, P.S. Ho, *MRS Bulletin,* **22** (10), p. 19 (1997).

2. E.T. Ryan, A.J. McKerrow, J. Leu, P.S. Ho, *MRS Bulletin,* **22** (10), p. 49 (1997).

3. R.S. List, A. Singh, A. Ralston, G. Dixit, *MRS Bulletin,* **22** (10), p. 61 (1997).

4. W.E. Sawyer, A. Man, U.S. Pat 229, 335 (1880).

5. J.W. Aylsworth, U.S. Pat 553, 296 (1896).

6. A. DeLodyguine, U.S. Pats 575,002 and 575,668 (1897).

7. L. Mond, U.S. Pat 445, 230 (1881).

8. C.E. Morosanu, *Thin Films by Chemical Vapor Deposition*, Elsevier, NY (1990).

9. N. Goldsmith, W. Kern, *RCA Rev.*, **28**, p.153 (1967).

10. H.M. Manasevit, *J. Electrochem. Soc.*, **115**, p.434 (1968).

11. E. Takinawa, O. Takayama, K. Maeda, *Denki Kagaku*, **41**, p. 491 (1973).

12. W. Kern, *RCA Rev.*, **34**, p. 655 (1973).

13. H. F. Sterling, R.C.G. Swann, *Solid-State Electron.*, **8**, p. 653 (1965).

14. H.C. Theurer, *J. Electrochem. Soc.*, **108**, p. 649 (1961).

15. W.A. Emerson, *Solid State Technol.*, **1**, (10), p. 50 (1967).

16. W. Kern, *RCA Rev.*, **29**, p. 525 (1968).

17. P.H. Lee, M.T. Wauk, R.S. Rosler, W.C. Benzing, *J. Electrochem. Soc.*,**114**, p. 1824 (1977).

18. E.O. Ernst, D. Hurd, G. Seeley, P. Olshefski, Electrochem. Soc., Fall Meeting (1965).

19. V.S. Ban, *J. Cryst. Growth*, **17**, p. 19 (1972).

20. G. Eriksson, *Chemica Scripta*, **8**, p. 100 (1975).

21. D.W. Shaw, *J. Electron. Mater.*, **2**, p. 255 (1973).

22. V.S. Ban, *J. Electrochem. Soc.*, **125**, p. 317 (1978).

23. M.E. Coltrin, R.J. Kee, J.A. Miller, *J. Electrochem. Soc.*, **131** (2), p. 425 (1984).

24. M.E. Coltrin, R.J. Kee, J.A. Miller, *J. Electrochem. Soc.*, **133** (6), p. 1206 (1986).

25. P. N. Gadgil, *J. Electron. Mat.*, **22** (10), p. 171 (1993).

26. D.S. Dandy, J. Yun, *J. Mater. Res.*, **12** (4), p. 1112 (1997).

27. C. Houtman, D.B. Graves, K.F. Jensen, *J. Electrochem. Soc.*, **133**, p. 961 (1986).

28. J. Szekely, A.H. Dilwari, *J. Cryst. Growth*, **108**, p. 491 (1991).

29. S. Desu, S.R. Kalidindi, *Jap. J. Appl. Phys.*, **29** (7), p. 1310 (1990).

30. J. Gaynor, PhD. Dissertation, Virginia Polytechnic Institute and State University, Blacksburg, VA (1995).

31. J.J. Senkevich, S.Desu, *Thin Solid Films*, **322**, p. 148 (1998).

32. J.J. Senkevich, S.Desu, to be published in *Chemistry of Materials*, July 19, 1999.

33. M. Swarc, *Disc. Faraday Soc.*, **2**, p. 46 (1947).

34. M.H. Kaufman, H.F. Mark, R.B. Mesrobian, *J. Polym. Sci.*, **13**, p. 3 (1954).

35. R.S. Corley, H.C. Haas, M.W. Kane, D.I. Livingston, *J. Polym. Sci.*, **13**, p. 137 (1954).

36. W.F. Gorham, *J. Polym. Sci. Part: A-1*, **4**, p. 3027 (1966).

37. C.J. Brown, *J. Chem. Soc.*, p. 3265 (1953).

38. L. Errede, J. Hoyt, *J. Amer. Chem. Soc.*, **82**, p. 436 (1960).

39. C. Shief, D. McNally, R. Boyd, *Tetrahedron*, **25** (17), p. 3653 (1965).

40. D. Williams, J. Pearson, M. Levy, *J. Amer. Chem. Soc.*, **92** (5), p. 1436 (1970).

41. L. Montgomery, J. Huffman, E. Jurczack, M. Grendze, *J. Amer. Chem. Soc.*, **108**, p. 6004 (1986).

42. W. Beach, T. Austin, 3rd. *Intl. SAMPE Elec. Conf., Elec. Mat. Proc.*, p. 78 (1989).

43. L. Aleksandrova, *Polymer*, **35** (21), p. 4656 (1994).

44. S. Isoda, *Polymer*, **25**, p. 615 (1984).

45. P. Kramer, A. Sharma, E. Hennecke, H. Yasuda, *J. Polym. Sci., Polym. Chem.,* **22**, p. 475 (1984).

46. M. Gazicki, G. Surendran, W. James, H. Yasuda, *J. Polym. Sci., Polym. Chem.,* **23**, p. 2255 (1985).

47. M. Gazicki, G. Surendran, W. James, H. Yasuda, *J. Polym. Sci., Polym. Chem.,* **24**, p. 215 (1986).

48. G. Surendran, M. Gazicki, W. James, H. Yasuda, *J. Polym. Sci., Polym. Chem.,* **25**, p. 1481 (1987).

49. G. Surendran, M. Gazicki, W. James, H. Yasuda, *J. Polym. Sci., Polym. Chem.,* **25**, p. 2089 (1987).

50. A. Sharma, *J. Polym. Sci. A, Polym. Chem.,* **26**, p. 2953 (1988).

51. W. Beach, *Macromolecules*, **11** (1), p. 72 (1978).

52. J. Gaynor, PhD. Dissertation, Virginia Polytechnic Institute and State University, Blacksburg, VA (1995).

53. W.D. Niegisch, *Poly. Lett.*, **4**, p. 531 (1966).

54. W.D. Niegisch, *J. Appl. Phys.*, **37** (11), p. 4041 (1966).

55. W.D. Niegisch,, *J. Appl. Phys.*, **38** (11), p. 4110 (1967).

56. S. Kubo, J. Wunderlich, *J. Appl. Phys.*, **42** (12) p. 4558 (1971).

57. S. Kubo, J. Wunderlich, *J. Appl. Phys.*, **42** (12) p. 4565 (1971).

58. S. Kubo, J. Wunderlich, *Die Makromole. Chemie*, **162** p. 1 (1972).

59. S. Kubo, J. Wunderlich, *Die Makromole. Chemie*, **157** p. 299 (1972).

60. S. Isoda, M. Tsuji, M. Ohara, A. Kawaguchi, K. Katayama, *Polymer*, **23**, p. 1568 (1982).

61. S. Isoda, M. Tsuji, M. Ohara, A. Kawaguchi, K. Katayama, *Polymer*, **24**, p. 1155 (1983).

62. S. Isoda, *Polymer*, **25**, p. 615 (1984).

63. See ref. 52.

64. M. Kobayashi, *Polym. Lett.*, **8**, p. 823 (1970).

65. M. Gazicki, W.J. James, H.K. Yasuda, *J. Polym. Sci.: Polym. Lett. Ed.*, **23**, p. 639 (1985).

66. J.F. Gaynor, S. Desu, *J. Mater. Res.*, **11** (1), p. 236 (1996).

67. J.F. Gaynor, S. Desu, *J. Mater. Res.,* **9** (12), p. 3125 (1994).

68. J.F. Gaynor, S. Desu, J.J. Senkevich, *Macromolecules*, **28**, p. 7343 (1995).

69. J.F. Gaynor, S. Desu, J.J. Senkevich, *J. Mater. Res.*, **11** (7), p. 1842 (1996).

70. M. Swarc, *Polym. Eng. Sci.*, **16** (7), p. 473 (1976).

71. W.F. Beach, C. Lee, D.R. Bassett, T.M. Austin, R. Olson, *Encycl. Polym. Sci. & Eng.*, **17**, Wiley & Sons, New York (1989), p. 990.

72. R. Olson, *Proc. 19th Electrical/Electronics Insul. Conf.*, p. 272 (1989).

73. S. Jeng, M. Chang, T. Kroger, P. McNally, R. Havemann, *Symp. VLSI Technol. Digest Tech. Papers*, p. 73 (1994).

74. C. Val, M. Leroy, J. Chambre, D. Bourret, R. Sempere, A. Doucoure, *11th IEEE/CHMT European International Electronic Manufacturing Technology Symposium*, p. 356 (1991).

75. B. Bachman, *Proc. 1ˢᵗ Intl. SAMPE Electronics Conf.*, p. 431 (1987).

76. G. Loeb, M. Bak, M. Salcman, E. Schmidt, *IEEE Trans. Biomed. Eng.*, **BME-24** (2), p. 121 (1977).

77. K. Stephan, H. Brauninger, C. Reppin, H. Maier, D. Frischke, M. Krumrey, P. Muller, *Nucl. Inst. Meth. Phys. Res. A*, **28**, p. 289 (1994).

78. J. Wary, R. Olson, W. Beach, *Semiconductor International,* **19** (6), p. 211 (1996).

79. R. Sutcliffe, W.W. Lee, J.F. Gaynor, J.D. Luttmer, D. Martini, J. Kelber, M.A. Plano, *Appl. Surf. Sci.,* **126** (1-2), p. 43 (1998).

80. A.S. Harrus, M.A. Plano, D. Kumar, J. Kelly, *Mat. Res. Soc. Symp.*, **443**, p. 21 (1997).

81. M.A. Plano, D. Kumar, T.J. Cleary, *Mat. Res. Soc. Symp.*, **476**, p. 213 (1997).

82. J.J. Senkevich, S. Desu, *Chemical Vapor Deposition*, **4** (3), p. 92 (1998).

83. J.J. Senkevich, S. Desu, *Thin Solid Films*, **322**, p. 148 (1998).

84. W.E. Wallace, J.H. van Zanten, W.L. Wu, *Phys. Rev. E*, **52** (4), p. R3329 (1995).

85. R.D. Miller, J.L. Hedrick, D.Y. Yoon, R.F. Cook, J.P. Hummel, *MRS Bulletin,* **22** (10), p. 44 (1997).

86. J.L. Hedrick, S. Srinivasan, H.J. Cha, D. Yoon, V. Flores, M. Harbison, *Mat. Res. Soc. Symp.*, **443**, p. 47 (1997).

87. C. Sanchez, A. Lafuma, L. Rozen, *Proceedings of the SPIE*, **3469**, p. 192 (1998).

88. L. Xiaochun, T.A. King, *J. Sol-Gel Sci. & Tech.*, **4** (1), p. 75 (1995).

89. I. Hasewaga, T. Takayama, S. Naito, *MRS Bulletin,* **34** (1), p. 63 (1999).

90. S. Matakef, T. Suratwala, R.L. Roncone, *J. of Non-Crystal Solids*, **178**, p. 37 (1994).

91. See ref. 69.

92. J.T Kelly, M. Eissa, J.F. Gaynor, S.P. Jeng, H. Nguyen, *Mat. Res. Soc. Symp. Proc.*, **476**, p. 197 (1997).

93. See ref. 32.

94. S. Desu, C.H. Peng, T. Shi, P.A. Agaskar, *J. Electrochem. Soc.*, **139** (9), p. 2682 (1992).

95. M.D. Nyman, S. Desu, C.H. Peng, *Chem. Mater.*, **5**, p. 1636 (1993).

96. J. N. Bremmer, Y. Liu, K.G. Gruszynski, F.C. Dall, *Mat. Res. Soc. Symp. Proc.*, **476**, p. 37 (1997).

97. V.P. Korchov, T.N. Martynova, V.I. Belyi, *Thin Solid Films*, **101**, p. 373 (1983).

ELLIPSOMETRY DATA

The quality and reliability of data in any scientific work must be taken into consideration when interpreting the results. The following section explains the data collected by the variable angle spectroscopic ellipsometer which was used for the determination of film thickness as well as the index of refraction. Since both the thickness and the index of refraction are based on a model fit of the raw data, examples of raw data collected by the instrument are presented along with the resulting fit.

The ellipsometer collects information about elliptically polarized light reflected from the surface of a film. Monochromatic elliptically polarized light that is reflected from a surface experiences a polarization rotation and a phase shift, leading to changes in the perpendicular and in-plane electric field components. The extent of this change is recorded by the detector in terms of two angles, Ψ and Δ, which depend on the optical properties of the film as well as its thickness. The film needs to be on a substrate with high reflectivity, thus substrates in this work were either single crystal silicon or platinum. Data was collected for wavelengths from 400 to 1000 nm, thus covering the whole visible spectrum, at three different angles of incidence. The angles of incidence depended on the Brewster's angle for the film material, and were 60, 65, 70 $^{\circ}$ for parylene films, and 65, 70, 75 $^{\circ}$ for SiO_2 or similar films. The equations used to compute the thickness and index of refraction as well as the extinction coefficient are given below:[1]

$$2\Psi - 2\Psi_0 = \text{Sin } 2 \; \{(\beta \, 4 \, \text{Cos } \theta \, \text{Sin}^2 \, \theta)/(\text{Cos}^2\theta - \alpha^2) + \beta^2)\}(1 - n^2 \, \text{Cos}^2\theta)(1-n^{-2})t$$

$$\Delta_0 - \Delta = \{(\text{Cos}^2\theta - \alpha) \, 4 \, \text{Cos}\theta \, \text{Sin}^2\theta)/((\text{Cos}^2\theta - \alpha)^2 + \beta^2)\}(1 - n^{-2})t$$

$$\alpha = (1 - (k/n)^2/(n^2(1 + (k/n)^2)) \qquad \beta = (2k/n)/(n^2(1 + (k/n)^2)^2$$

where θ is the angle of incidence, t is the films thickness, and n and k are the index of refraction and extinction coefficient, respectively. These are the equations used to convert the raw data such as shown in the figures below to meaningful parameters. The models chosen for n and k were based on successful previous experience from past research in this area.[2] For isotropic films, the Cauchy model was utilized, which is based on the empirical relation

$n = A + B/\lambda^2 + C/\lambda^4$, where A, B and C are constants. The extinction coefficient relation is $k = k_0\, e^{(hc/\text{Band Edge} - hc/\lambda)}$. For birefringent films, the anisotropic Cauchy model was used, with $n_1 = A_n + B_n/\lambda^2$ and $n_2 = A_k + B_k/\lambda^2$. The thickness nonuniformity was modeled as well, with a squuare convolution profile using 5 points. The parameters which were thus fitted to the experimental data for the Cauchy model were A, B, C, k, the thickness, and the thickness nonuniformity. For the anisotropic Cauchy model, the parameters that were fitted were A_n, B_n, A_k, B_k, the thickness, and the thickness nonuniformity. Figures 1 through 4 below show typical data gathered by the ellipsometer. The dashed lines in the figures represent the experimental data for the three angles of incidence. The solid lines are the model fit for the three angles. The data for the polymer show an excellent fit, and the mean square error (MSE) of the fit for polymer films ranged from 5 to 40. A fit with an MSE of less than 40 was considered very reliable. Figure 2 shows data for an SiO_2
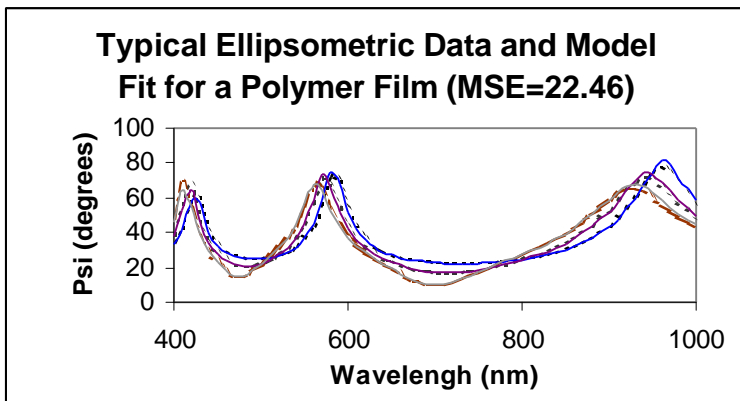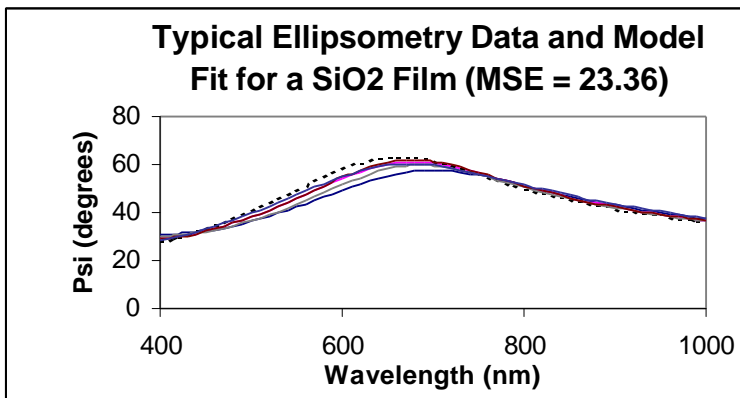

Figure 1

Figure 2

Ellipsometry Data and Model Fit for a Vinyl-T8 Film (MSE = 85.91)

Figure 3

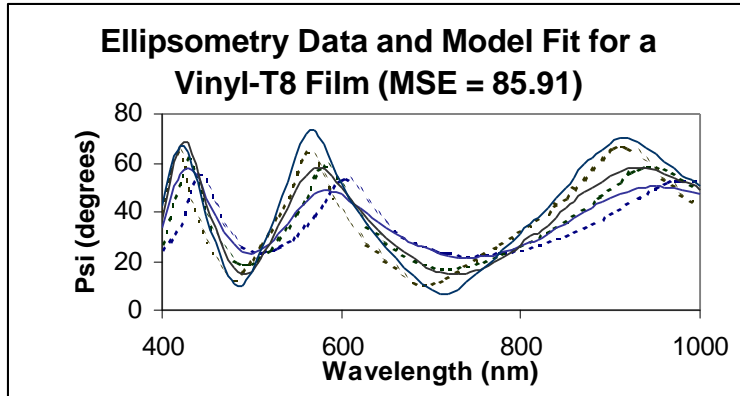**Elliipsometry Data and Model Fit for a very thick Vinyl-T8 Film (MSE = 97.4)**
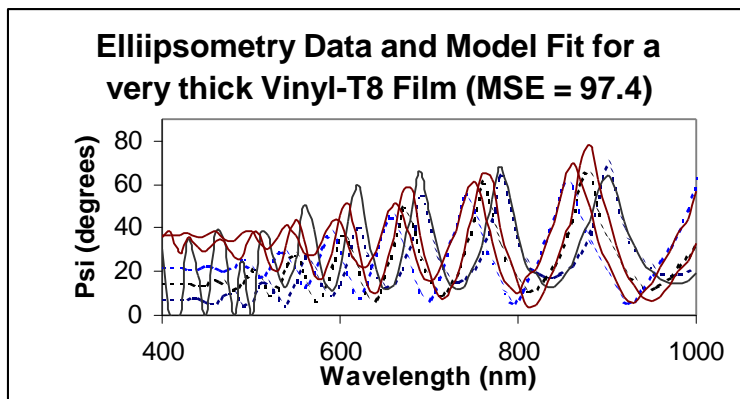
Figure 4

film. The fit is again very reliable. Silica films could be fitted well, although the MSE tended to a little higher than for parylene films. This was probably due to larger surface roughness and porosity. Figure 3 shows data for a vinyl-T8 film, with an MSE of 85.91. This data was chosen for illustration as it shows one of the worst fits that was considered acceptable. An MSE value of between 40 and 100 was accepted with the knowledge that considerable care must be taken in the interpretation of the results. Any MSE over 100 was rejected. Figure 4 show the data for a very thick film, and it can be seen that for films over 2000 nm in thickness, difficulty in fitting the data arises from the multitude of maxima and minima in the Psi curve. Repeated measurements and fits for films with MSEs of the fit between 40 and 100 tended to yield results within a standard deviation of the mean, and thus the fiits were deemed credible.

References

1. Woolam, Snyder, Johs, *Long Wavelength Semiconductor Deviices, Materials, and Processes. Symp. Mat. Res. Soc.*, (**543**), 1991, p. 459.

2. J. Gaynor, PhD. Disseration, Virginia Tech (1995).

Chapter 1

Scale-Up Study of a Modified CVD Reactor

Abstract

A modified CVD reactor was designed with a deposition chamber capable of accomodating 8" wafers, with the capacity to remotely pyrolyze two different precursors. The design was based on a previous working reactor, with the most notable improvements being a showerhead design for more even delivery of gaseous precursor and a separate heating control of the substrate holder and deposition chamber walls. The performance of the reactor was analyzed by testing the pressure gradients within and the thickness uniformity of films deposited on 8" wafers. The reactor exhibited a linear pressure gradient within, and the thickness uniformity was excellent, with a slight increase in thickness towards inlet of the showerhead. The thickness difference between the maximum and minimum thickness on an 8" wafer was 14%. Films of PPXN, PPXC, SiO_2, and $PPXC/SiO_2$ were deposited, with deposition rates and indices of refraction comparable to those obtained on the old reactor design. A full factorial study was performed to determine the effect of the substrate temperature, the sublimation temperature, and the pyrolysis temperature on the deposition rates of PPXC. It was determined that the substrate temperature has the greatest effect, with about 50% contribution, and deposition rates increased with decreasing substrate temperature. The sublimation temperature contributed 25%, with increasing sublimation rates leading to higher deposition rates. The pyrolysis contributes very little, with about 2%, and the variance ratio did not fall within a 90% confidence level.

Introduction

Chemical vapor deposition (CVD) has become the dominant processing technique in the semiconductor industry. In CVD, the film forms on the substrate by means of a chemical reaction that occurs at the substrate surface. A reactive intermediate needs to reach the substrate surface in the gas phase from a precursor source. CVD offers many advantages over physical deposition techniques such as evaporation or sputtering. The main benefit derived by a CVD process is the result of a uniform, adherent, reproducible film with excellent step coverage. Step coverage is a measure of how uniformly a film forms on geometry with high aspect ratios such as vias and trenches. The main disadvantages lie in the need to oftentimes resort to dangerous and toxic chemicals to obtain the desired material along with the high temperatures necessary for some of the reactions.[1]

A CVD reactor consists of three functional components: a system for generating and delivering sufficient concentrations of the gaseous reactants to the substrate, a system for housing the substrate and providing the necessary conditions for the reaction to occur, and a system for maintaining the vacuum and removing the by-products of the reaction. Typically, the reactants are generated from a precursor which is either evaporated or sublimed into the gaseous state. If the vapor pressure of the precursor is low, an inert carrier gas such as N_2 or Ar is introduced. Generation of the reactive species from the sublimed precursor can be accomplished by various means. The most common techniques are thermally induced CVD, plasma enhanced CVD, laser assisted CVD, and electron beam assisted CVD. The pressure and concentration gradients drive the reactants into the area of the reactor where the substrate is housed, leading to film formation on the substrate if the deposition conditions are right. The by-products of the reaction as well as unused reactants then travel towards the exhaust system, which usually consists of a cold trap and the pumping mechanism.[2]

Reactor Design and Description

A schematic diagram of the reactor designed and build for this work is shown below. Photographs of the reactor are shown on the next page in Figs 2 and 3. This design is an improvement over an earlier system which has been used previously for similar research.[3]
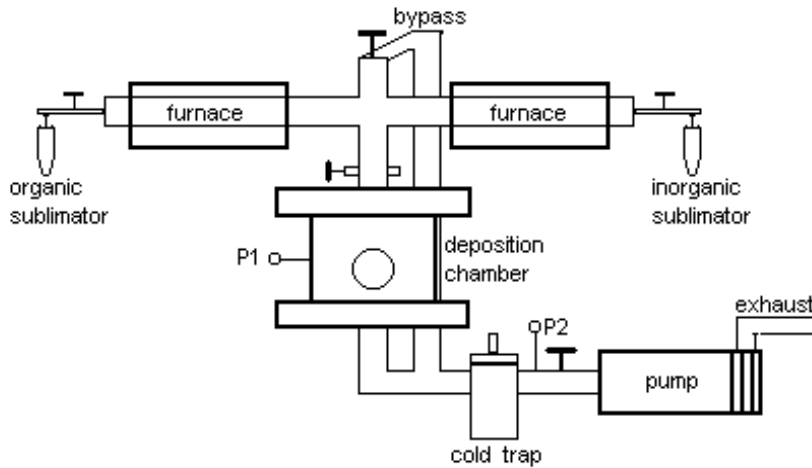

Figure 1 – Schematic Diagram of the Reactor

The specific improvements are discussed later. The system was designed for depositions of nanocomposites consisting of two different phases, utilizing two precursors with different pyrolysis requirements. Both sides, one of which supplies the organic phase precursor, and one the inorganic phase, have the same structure. The sublimation chambers were either steel or quartz (depending on whether the precursor was solid or liquid), 1.5" in diameter and 5" long. The chambers were attached to the tubing leading to the pyrolysis furnace with Viton O-ring seals. The temperature was monitored with a K-type thermocouple attached to the outside bottom of the sublimation chamber and
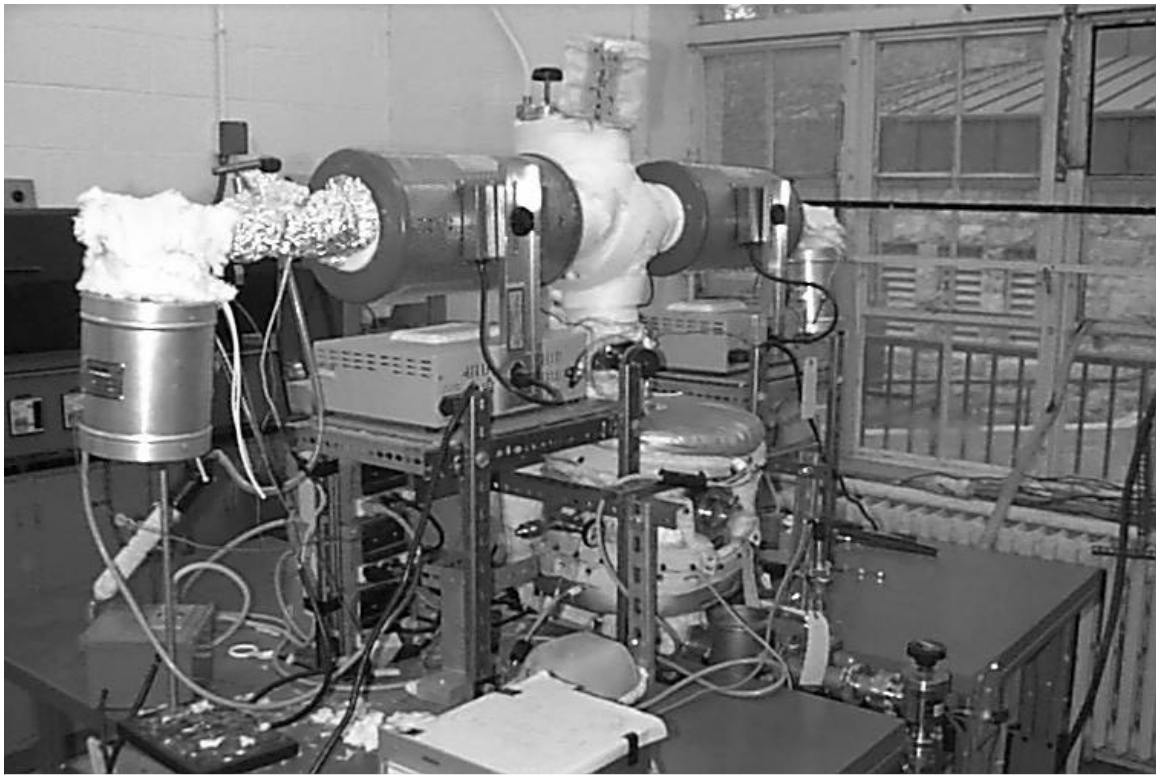
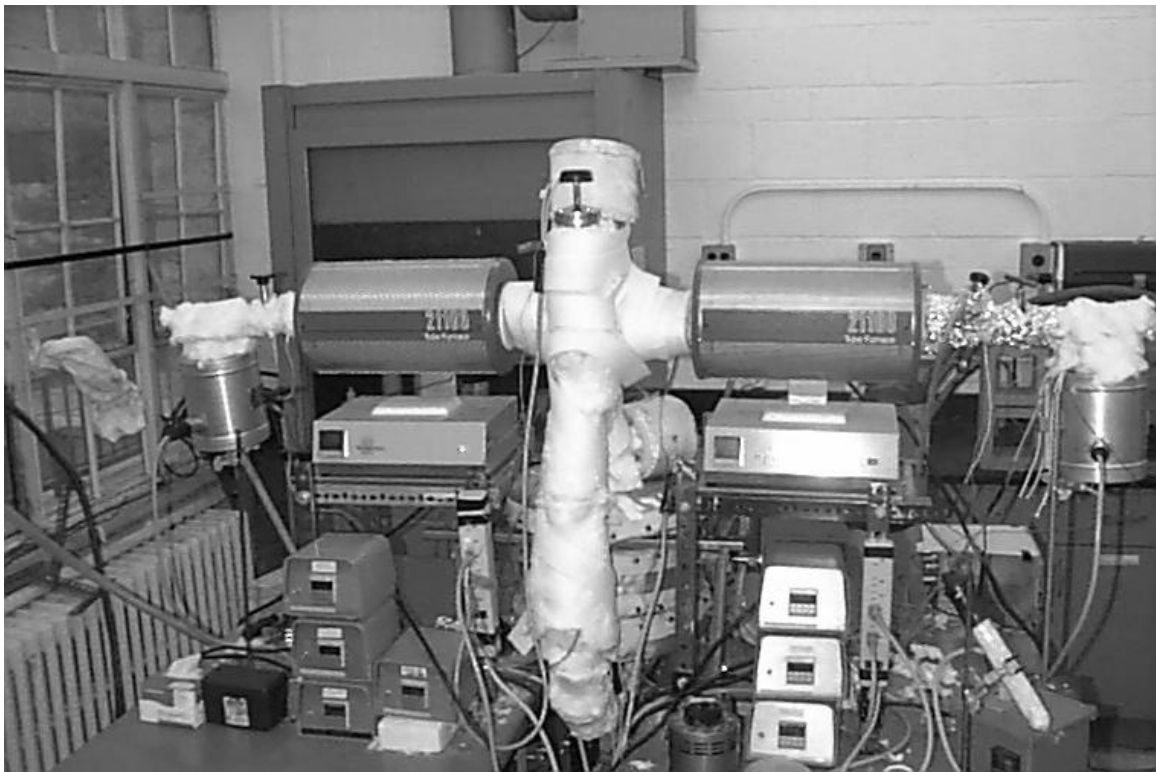**Figure 2 – Front View of the Reactor**

Figure 3 – Back View of the Reactor

connected to a 15A, 125V Teco temperature controller. The heating was provided by a heating mantle provided by Glas-Col[1]. It was discovered that the heating from the mantle was nonuniform, providing more heat to the bottom of the sublimation chamber. This caused a cold spot towards the top of the chamber leading to recondensation of the precursor. The problem was solved by winding a short 1' heating tape around the top of the sublimation chamber.

The sublimation chambers were connected to the pyrolysis furnaces with ½" metal tubing using Swagelock connectors. A valve placed between the sublimation chamber and the furnace controlled the flow of the sublimed precursor gas. The temperature of the tubing from the chamber to the furnace was controlled with another Teco controller, connected to a K-type thermocouple attached to the tubing with a metal hose clamp and heating tapes wound around the tubing.

The pyrolysis chamber was custom built from 2" OD Inconel tubing to which a Swagelock connector was welded on the input side, and a 3 3/8" CF flange was welded on the output side. The heating of the pyrolysis chambers was accomplished with Thermolyne 21100 furnaces. The pyrolysis chambers experience temperatures of up to 700 ^{o}C for extended periods of time. Steel undergoes significant oxidation at these temperatures, which leads to the formation of flakes on the inside surface. These flakes provide an undesirable increase in surface area on which the generated reactive intermediate can deposit, leading to a lowered concentration and thus lower deposition rates within the deposition chamber. To mitigate this problem, Inconel tubing, which has high oxidation resistance, was used. Past research has indicated that the introduction of a baffle into the chamber, which significantly slows down the gas flow within the chamber, leads to a higher percent conversion of the pyrolysis reaction.[4] Previous designs utilized a metal baffle consisting of semicircular plates bolted together with the flat sides at 45° to each other, forcing the gas into a spiral flow around them. To minimize oxidation and further increase the residence time of the precursor in the furnace, quartz 5" long hollow

---

[1] (711 Hulman St., PO Box 2128, Terre Haute, IN 47802, 812-235-6167)

cylinders, which fit snugly inside the tubing and were filled with ½" long, ¼" diameter glass tubing pieces, were custom built and used as baffles.

The two pyrolysis chambers were attached with 3 3/8" Del-Seal flanges to a 4-way cross, which is where mixing of the two gas phases occurred. Temperature of the cross region was measured with a K-type thermocouple connected to a Teco controller and heated with 3.5 A heating tapes. Everywhere where heating tapes were used on the reactor, they were covered with fiberglass insulation to maximize heating efficiency and reduce the risk of exposure to high temperature surfaces for the operator. The cross was connected to the bypass as well as the deposition chamber. A right angle valve from MDC controlled flow into the bypass tube while a MDC CU-1500M gate valve controlled the flow into the deposition chamber. The bypass tube led to a T connector, where it met up with the exit port of the deposition chamber and connected to the cold trap. The purpose of the bypass tube was to prevent the initial surge of the gaseous reactant from entering the deposition chamber and reacting on the substrate. Only after steady-state conditions were achieved was the valve to the deposition chamber opened and the valve to the bypass closed.

The deposition chamber was supplied by Quester Technologies of Fremont, CA and was designed to accommodate 8" wafers. The inside measurements of the cylindrical chamber were 8" in diameter and 6" in height. The entry port was a 1" diameter tube, which was a design flaw, since this restricted the throughput. The top of the chamber had a showerhead design so that the incoming gases were redistributed from the entry port uniformly throughout the top of deposition chamber, resulting in minimum turbulence and uniform flow. The bottom of the chamber was covered with the substrate holder, which was hollow with two ports, allowing either heating or cooling by a liquid. A Polyscience model 9705 circulator, with cooling capacity of up to $-40\ ^{\circ}C$, was used for this purpose. The liquid used for the cooling was a 50/50 mixture of water and propylene glycol. This was not the ideal fluid, since at temperatures below $0\ ^{\circ}C$, the viscosity became too high for efficient circulation, but was used due to financial constraints. Three additional ports besides the entry and exit ports for the gases were present on the

deposition chamber. On the top was a 1" port which housed an electrical feedthrough connected to two K-type thermocouples. One measured the temperature inside the showerhead, while the other measured the temperature of the top of the substrate holder. A port on the side of the chamber was connected to a MKS Baratron type vacuum gauge. This gauge later went out of calibration and due to financial constraints was not used in the later parts of this work. Finally, on the side of the chamber facing the front was a 1.5" diameter glass port which was used to insert and remove samples from the reactor. For the deposition of whole wafers, the bottom or top of the chamber had to be removed.

Temperature control of the deposition reactor was crucial. This was accomplished with custom built heating mantles provided by Glas-Col and Teco temperature controllers. Three heating zones were established. The top of the chamber, including the showerhead, was the first zone. The second zone included the sides as well as the bottom of the reactor, for which the K-type thermocouple was attached to the outside wall of the reactor chamber. The third zone was the area of the sample insertion port, for which a separate heating mantle was used due to geometric constraints. The temperature control zones for the whole reactor are shown below.
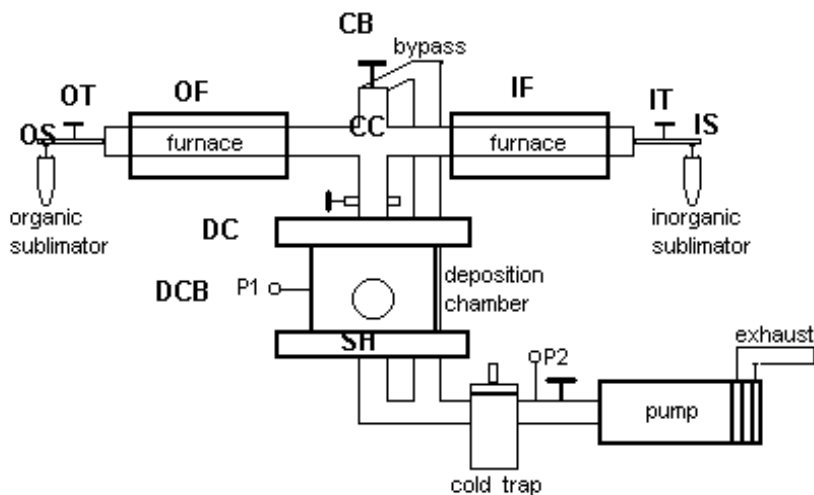
OS = *organic sublimator,* *OT* = *tubing from organic sublimator to organic furnace,* *OF* = *organic furnace,* *IS* = *inorganic sublimator,* *IT* = *tubing from inorganic sublimator to inorganic furnace,* *IF* = *inorganic furnace,* *CB* = *cross and bypass,* *CC* = *cross to deposition chamber tubing,* *DC* = *deposition chamber top (showerhead),* *DCB* = *deposition chamber body,* *SH* = *substrate holder*

Figure 4 – Diagram of the temperature zones in the reactor

The T connector which united the bypass tube and the exit port of the deposition chamber led to the liquid nitrogen cold trap. The main function of the cold trap was to trap all the by-products of any deposition, thus preventing damage to the pump as well as pollution of the air. Another vacuum gauge was located after the cold trap, connected to a Pirani GP-2TRY analog vacuum gauge unit. This gauge was used to measure the base pressure, which was consistently found to be 20 mTorr lower than the pressure inside the deposition chamber. The system was then connected to an Alcatel T2033CP1 mechanical pump, which provided pressures of 25-150 mTorr. It took about 1 minute with this pump to pump down to the base pressure. The vent of the system was located on the tubing leading from the sublimation chamber to the pyrolysis furnace.

During the course of this research, the reactor underwent several design changes. Initially, the pathway from the pyrolysis furnaces to the deposition chamber involved too many bends and turns, which lead to Hamel backflow and possible turbulence.[5] This is undesirable as not only does it slow down gas flow and decrease throughput, but it also leads to deposition of the reactive species at the location of the bends, thus decreasing their actual concentration in the deposition chamber. Therefore, the design of the reactor was such that the path from the formation of the reactants in the furnace to the substrate was the shortest and straightest possible.

It was stated previously that the reactor design was an improvement over a design used in previous research. The specific improvements will now be enumerated. The old reactor could accommodate wafers of up to 6" in diameter, while the new reactor was designed for 8" wafers. This was the main motivation for the new reactor, providing a scale-up study of the research performed previously. The flow into the old reactor was not controlled, while the new reactor ensured uniform flow through the showerhead design. The walls of the old reactor and the substrate had to be kept at the same temperature, as no separate temperature control was provided for the substrate. Furthermore, the temperature of the deposition chamber was maintained with a circulating liquid, which led to substantial heat loss and inefficiency. Overall, the new design included a more

precise control of the temperature gradients within different parts of the reactor, which is crucial for successful chemical vapor deposition. The tubing used for the furnaces of the old reactor was made of steel, as were the baffles, leading to the need for frequent cleaning due to the formation of flakes caused by severe oxidation of the steel. Finally, the old reactor had only one pressure gauge, thus pressure gradients could not be determined. This was remedied on the new reactor.

Reactor Performance

Several characteristics of the reactor were essential to proper performance. The gas flow within the reactor is controlled by two gradients, namely the pressure gradient caused by the vacuum, and the concentration gradient of the precursor. A study was done on the effect of the gas flow rate on pressure. Dry nitrogen gas was introduced into the system through the sublimation chamber and the flow of the gas was controlled by a MKS flow controller. The base pressure in the system achieved by the pump was plotted
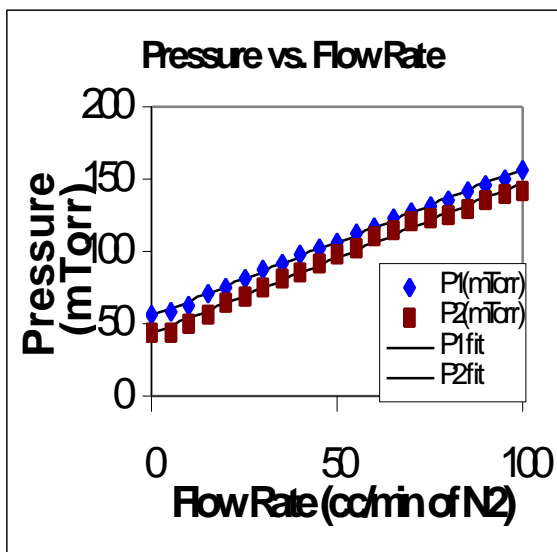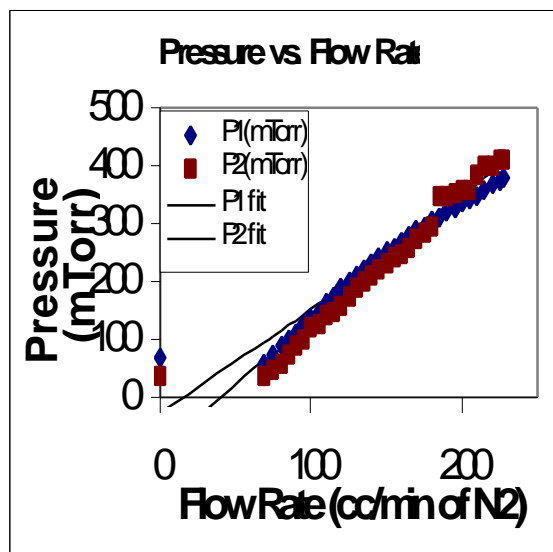
Figure 5 – Flow rate in the reactor

Figure 6 – Flow rate in the reactor

as a function of the gas flow rate for flow meters calibrated for two different scales. Figures 5 and 6 show that the pressure increased linearly with increasing gas flow. This

linear relationship is desirable, as not only can the gas flow rate be estimated from a measured pressure, but any variations such as changes in the reactor leak rate, pump performance, temperature distribution, or the reactor internal surface area, will lead to small changes in the gas flow rate. Unpredictable nonlinear deviations from the gas flow rate within the reactor are therefore very unlikely. The pressure within the deposition chamber was measured by pressure gauge P1, while the base pressure was measured right before the pump by gauge P2. Both figures show a consistent difference between the readings of the two gauges of 20 mTorr. This indicates that the pressure gradient within the reactor is relatively constant.

Thickness uniformity along a wafer is essential for consistent and reliable results. To test the film uniformity achievable in the reactor several 8" wafers were deposited. The films were poly(chloro-p-xylylene), or PPXC. The results of two depositions are shown below in Figures 7 and 8. The thickness was measured with a variable angle spectroscopic ellipsometer from J. Woollam Co. using an empirical anisotropic Cauchy equation. Due to geometric constraints, the thickness was measured up to 6.5" from the edge. The average thickness variations for the two wafers were 64 nm, or 4.9%, and 23 nm, or 3.5%. For the first wafer, the thickness rose from 2481 nm to 2812 nm, with an average thickness of 2631 nm and standard deviation of 126 nm. The thickness of the
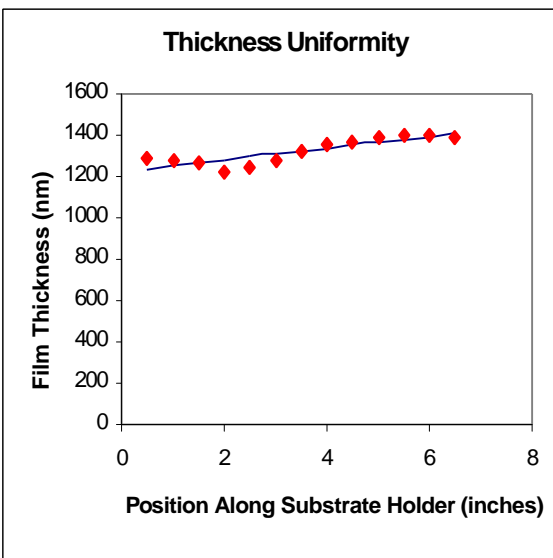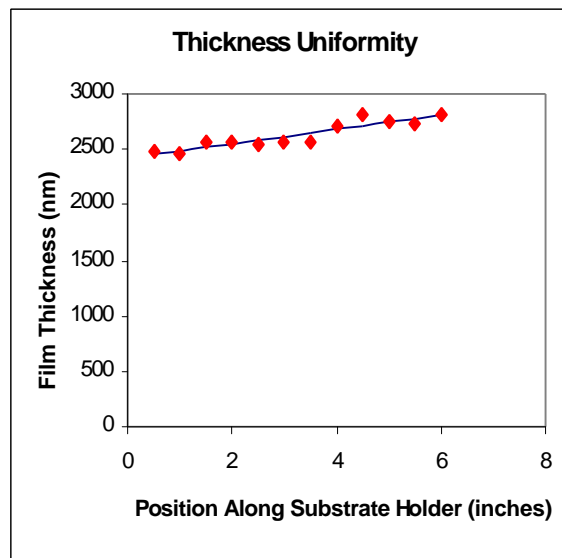

Figure 7 – Thickness Uniformity

Figure 8 – Thickness Uniformity

second wafer rose from 1263 nm to 1399 nm, with an average of 1325 nm and standard deviation of 67 nm. The overall thickness uniformity is thus very good, with a gradual increase in thickness towards the right side of the figures. This side represents the side closer to the inlet port of the deposition chamber. Therefore, while the showerhead is efficient in redistributing the gas flow uniformly throughout the top of the chamber, this redistribution is not complete and more reactant reaches the substrate on the side closer to the inlet port. Least square fits through the thickness measurement data yielded an equation for the thickness as a function of position along the substrate holder. Normalized for thickness, where t_0 is the thickness at x=0, the equation is $t = t_0/42*x + t_0$. As the new reactor was a scale-up model of the previous design, reproduction of old results was needed to compare the performance of the new reactor with the smaller, older model. Several materials were deposited for which data were available from previous work on the old reactor. Poly-para-xylylene, or PPXN, was deposited from cyclo-di-para-xylylene, followed by poly-chloro-p-xylylene (PPXC) from cyclo-di-chloro-p-xylylene, and poly-dichloro-p-xylylene (PPXD) from cyclo-di-dichloro-p-xylylene. The properties and processing conditions of these polymeric materials are well established. SiO_2 was deposited next, from the precursor di-acetoxy,di-butoxysilane, or DADBS. This unique low temperature deposition process was first developed on the old reactor.[6] Nanocomposite films of PPXC and SiO_2 were also successfully deposited, and the phase composition could be controlled by controlling the sublimation and vaporization rates of the two precursors. The table below summarizes the results obtained for the films of these materials for typical deposition conditions. The index of refraction and deposition rate values are comparable to those obtained on the old reactor. The only discrepancy is

Material	Dep. Rate (nm/min)	n1	n2
PPXN	15.3	1.66	1.59
PPXC	14.8	1.66	1.63
		N	k
SiO2	2.5	1.41	0.0024
		n (26% PPXC)	n (93 % PPXC)
PPXC/SiO2	4.3	1.49	1.63

Table 1 – Films Deposited Using New Reactor Design

the fact that the deposition rates for SiO_2 films were higher for the old reactor, on the order of 10 nm/min.[7] This was due to the shorter pathway of the reactive intermediate species. A full factorial study was performed with PPXC in order to determine the deposition kinetics. The three factors that contribute the most to the deposition rate were studied, each at four levels. The sublimation temperature (OS) of the precursor determines the vapor pressure and was thus postulated to have the greatest effect on the deposition rate. The substrate temperature (SH) determines the rate of condensation of the reactants onto the substrate where polymerization occurs, and thus has a great effect on the deposition rate. Finally, the pyrolysis temperature (OF) controls the rate at which the reactive species is generated from the precursor, and thus affects the concentration of the reactant and the deposition rate. The deposition conditions were OS = 125, 130, 135, and 140 ^{o}C, OF = 600, 625, 650, 700 ^{o}C, and SH = 50, 25, 2 ^{o}C, for a total of 48 experiments. Figures 9-11 below show the results of this study along with least square fits. The general trend observed for a given pyrolysis temperature and substrate temperature was a linear increase in the deposition rate with increasing sublimation temperature. Individual data points, however, showed deviation from this trend, indicating a large experimental variance.
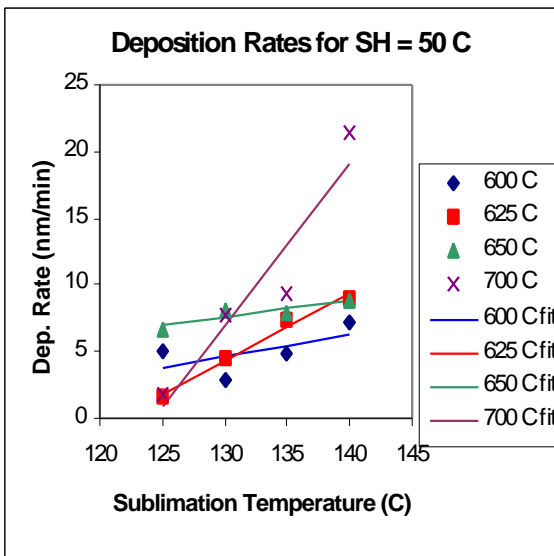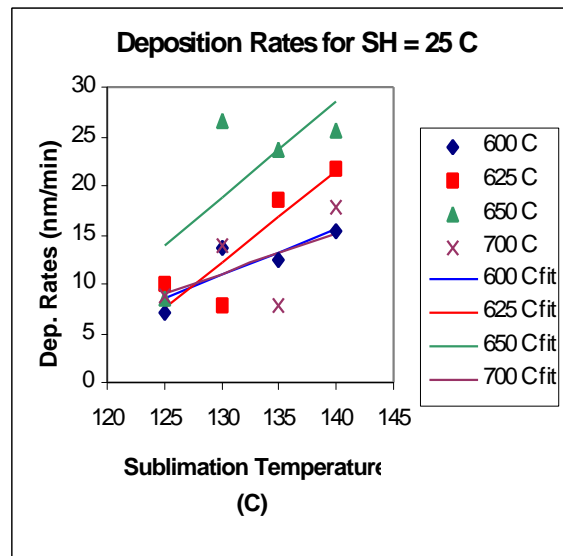

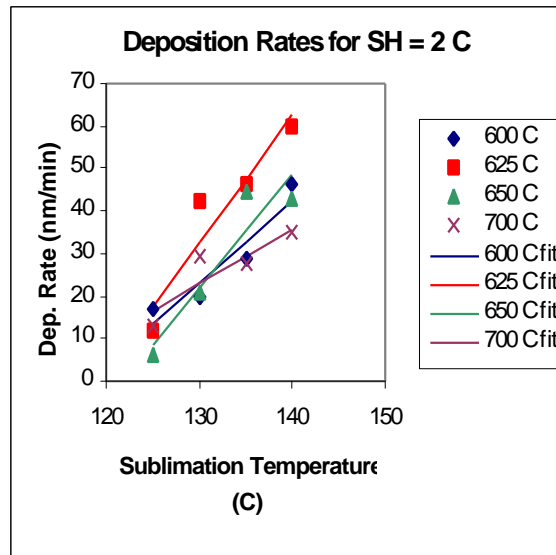Figure 9 – Dep. Rate for SH = 50 ^{o}C Figure 10 – Dep. Rate for SH = 25 ^{o}C

Figure 11 – Dep. Rate for SH = 2 $^{\circ}$C

The most significant effect on the deposition rate was from the substrate temperature, as can be seen by comparing the rates from the three figures. The pyrolysis temperature seems to have the least effect, and an increase does not guarantee higher deposition rates. These visual observations are substantiated by ANOVA analysis summarized in the tables below. The average performance of each factor at each level was computed by averaging the deposition rates for each experiment that included that factor level. From the table, it is obvious that the deposition rate increases with increasing sublimation temperature and decreasing substrate temperature, though the optimum pyrolysis temperature seems to be 625 $^{\circ}$C.

Substrate Temp.		Sublimation Temp.		Pyrolysis Temp.	
50 C	7.14	**125 C**	8.13	**600 C**	15.01
25 C	14.97	**130 C**	16.51	**625 C**	20.09
2 C	30.72	**135 C**	19.92	**650 C**	19.25
		140 C	25.89	**700 C**	16.10

Table 2 – Average performance at each factor level (Dep. Rates in nm/min)

The analysis of variance is given below in Table 3. Again, SH is the substrate temperature, OS is the organic sublimation temperature, and OF is the organic furnace, or pyrolysis temperature. The degrees of freedom for each factor are in the column labeled f, and are defined as the number of levels for that factor minus one. The total degrees of freedom are the number of trials performed minus one. The error degrees of freedom

Factors	F	S	V	F	P	F - 90%	F – 99%
SH	2	4612	2306	39	50.6%	2.4404	5.1785
OS	3	1979	660	11	21.7%	2.2261	4.3126
OF	3	215	73	1	2.4%	2.2261	4.3126
Error	39	2308	59	1	25.3%		
Total	47	9113			100%		

Table 3 – ANOVA results for the deposition rates study

are given by $f_e = f_t - f_{SH} - f_{OS} - f_{OF}$. Column S lists the sum of squares, while V is the variance, given by S_A/f_A. F is the variance ratio, defined as $F_A = V_A/V_e$. Finally, P is the percent contribution of each factor, given by $P_A = S_A*100/S_T$ and gives the contribution of each factor to the total. The last two columns are the standard F values from statistics tables for the given combination of degrees of freedom and given confidence level.[8,9] If the computed F value is less than the value determined from the F tables at the selected confidence level, the factor does not contribute to the sum of squares within that confidence level. Thus, SH, which has the greatest contribution, and OS, which also contributes greatly, are well within the confidence level for both 90% and 99%. OF, which has the least significant contribution, is also not within the confidence level, even at 90%. This data spread contributes 75% to the sample variability, while the remaining 25% variation, which represents the error term, is caused by other factors.

The new reactor, which enabled the processing of 8" wafers, incorporated several improvements over the previous design, most notable of which were a showerhead design for more uniform gas delivery, and a separate temperature control for the substrate holder and the deposition chamber walls. The pressure gradient within the reactor was shown to follow a linear profile and the thickness uniformity of the films was excellent, with a slight increase in thickness near the showerhead inlet side of the substrate holder. Films of PPXN, PPXC, SiO_2, as well as PPXC/SiO_2 nanocomposites with demonstrable compositional control were reproduced with deposition rates and index of refraction values comparable to the old reactor design. Finally, a full factorial study of the deposition rates of PPXC was performed to examine the effects of the substrate temperature, the sublimation temperature, and the pyrolysis temperature on the deposition

rate. It was found that the substrate temperature has the greatest effect, while the effect of the pyrolysis temperature is negligible.

REFERENCES

1. C.E. Morosanu, *Thin Films by Chemical Vapor Deposition*, Elsevier: Amsterdam (1990), p. 42.

2. C.E. Morosanu, *Thin Films by Chemical Vapor Deposition*, Elsevier: Amsterdam (1990), p. 345.

3. J.F. Gaynor, S. Desu, J.J. Senkevich, *J. Mater. Res.*, **11** (7), p. 1842 (1996).

4. J. Gaynor, PhD. Dissertation, Virginia Tech (1995).

5. J.L. Fitzjohn, W.L. Holstein, *J. Electrochem. Soc.*, **137** (2), p. 699 (1990).

6. J.J. Senkevich, S. Desu, *Chemical Vapor Deposition*, **4** (3), p. 92 (1998).

7. J.J. Senkevich, S.Desu, to be published in *Chemistry of Materials*, July 19, 1999.

8. J.S. Milton, J.C. Arnold, *Introduction to Probability and Statistics: Principles and Applications for Engineering and Computing Sciences 2nd ed.*, McGraw-Hill: New York, 1990.

9. R. Ranjit, *A Primer On the Taguchi Method*, Van Nostrand Reinhold: New York, 1990.

Chapter 2

VT-4: A New Low-k Polymer

Abstract

A low dielectric constant polymer, poly(tetrafluoro-*p*-xylylene) (VT-4), was synthesized by chemical vapor deposition from 4,5,7,8,12,13,15,16-octafluoro-[2.2]-paracyclophane (DVT-4). The main motivation was to find a cheaper alternative to AF-4 with similar properties. The dielectric constant of VT-4 was measured as 2.42 at 1 MHz, and the in-plane and out-of-plane indices of refraction were 1.605 and 1.47 at 630 nm. The large negative birefringence suggests a low out-of-plane dielectric constant, which is desired for interlayer dielectrics. The VT-4 polymer was found to be stable at 460 ^{o}C by TGA.

Introduction

Polymer materials deposited by chemical vapor deposition (CVD) are strong candidates for the low-k intermetallic material. The dielectric constant and the thermal stability are the two most important properties of any new dielectric incorporated into ULSI technology. While the dielectric constant should be as low as possible (<3), polymers that are thermally stable above 425 ^{o}C are necessary to withstand the metallization processing conditions. The class of polymers known as parylenes have been the most studied. Of these, poly(tetrafluoro-p-xylylene), or AF-4, with k = 2.28, has the best properties.[1-3] Flourine has the lowest polarizability and therefore replacing the hydrogen atoms with fluorine leads to a lower dielectric constant. This is also why polytetrafluoroethylene has to lowest dielectric constant possible for a polymeric material.[4] The precursors for AF-4, such as 1,1,2,2,9,9,10,10-octafluoro[2,2]-paracyclophane, are expensive and not easily available. Thus, a material with similar properties, yet inexpensive precursors, has been synthesized. Poly(tetrafluoro-p-xylylene), or VT-4, has been deposited from the dimer precursor 4,5,7,8,12,13,15,16-octafluoro-[2,2]-paracyclophane (DVT-4). The films were deposited in a modified CVD reactor using a procedure similar to that used to deposit the conventional parylenes like
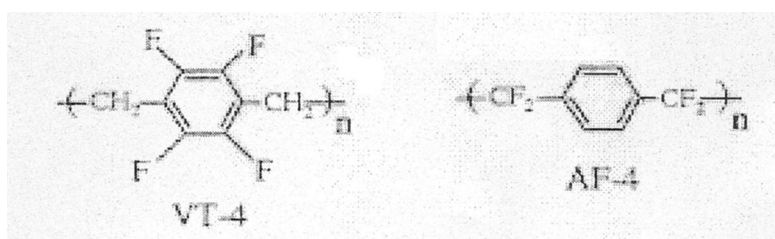

Figure 1 – Chemical Structure of VT-4 and AF-4

PPXN or PPXC. The chemical structure of both AF-4 and VT-4 is shown in Figure 1.

Experimental

The DVT-4 precursor, supplied by Koch Chemical Co., was sublimed at 115 ^{o}C, entering the pyrolysis chamber in the vapor state, where at a temperature of 650 ^{o}C decomposition into the diradical reactive intermediate took place. The diradical species then entered the

deposition chamber, where deposition and polymerization occurred on the substrate which was kept at 20 ^{o}C. The substrates used for deposition were (111) silicon polished on both sides for optical, XRD, and FTIR analysis, platinum substrates for dielectric analysis, and NaCl cells for TGA analysis, which were subsequently dissolved in a water bath to retrieve the film.

Optical measurements of film thickness and index of refraction were accomplished with a variable angle spectroscopic ellipsometer from J. Woollam Co. The samples were scanned at wavelengths from 400 to 1000 nm at angles of incidence of 60°, 65°, and 70°. Modeling was done using an anisotropic Cauchy model, based on the empirical equation $n = A + B/\lambda^2 + C/\lambda^4$, with the valid assumption that no absorption occurs in this wavelength range.[5] XRD analysis was performed with the Scintag XDS-2000 diffractometer at a rate of 2° 2θ/min. The FTIR spectrum was obtained with a Perkin Elmer model 1600 spectrometer. The dielectric constant and loss measurements were obtained with a Solarton SI 1260 Impedance Analyzer. The top platinum electrode, deposited by sputtering, had a circular area of 4.3-9.6 x 10^{-4} cm^2. Thermogravimetric analysis (TGA) was done using a Perkin Elmer analyzer under an argon atmosphere at a rate of 10 ^{o}C/min.

Results and Discussion

Figure 2 below shows the FTIR spectrum of a typical VT-4 film. The peaks at 2949 and 2875 cm^{-1} are from C-H alliphatic stretching. The strong peak at 1487 cm^{-1} results from the aromatic C-C stretch. Due to the presence of the electronegative fluorine atoms on the benzene rings, electrons are pulled away, thus weakening the C-C bond and causing a downward shift in wavenumber (this peak occurs at 1507 cm^{-1} for PPXN). The small peak at 1460 cm^{-1} results from the bending of the CH$_2$ group, while the larger peaks at 1301 and 1174 cm^{-1} are associated with C-F stretching on the benzene ring. The C-F stretching peaks for AF-4 are alliphatic, and therefore weaker, occuring at 1262 and 1146 cm^{-1}. Finally, at 938 cm^{-1}, a peak corresponding to the alliphatic C-C stretch

occurs.[6] The FTIR spectrum therefore demonstrates that the desired chemical structure, namely VT-4, was obtained in the depositions.
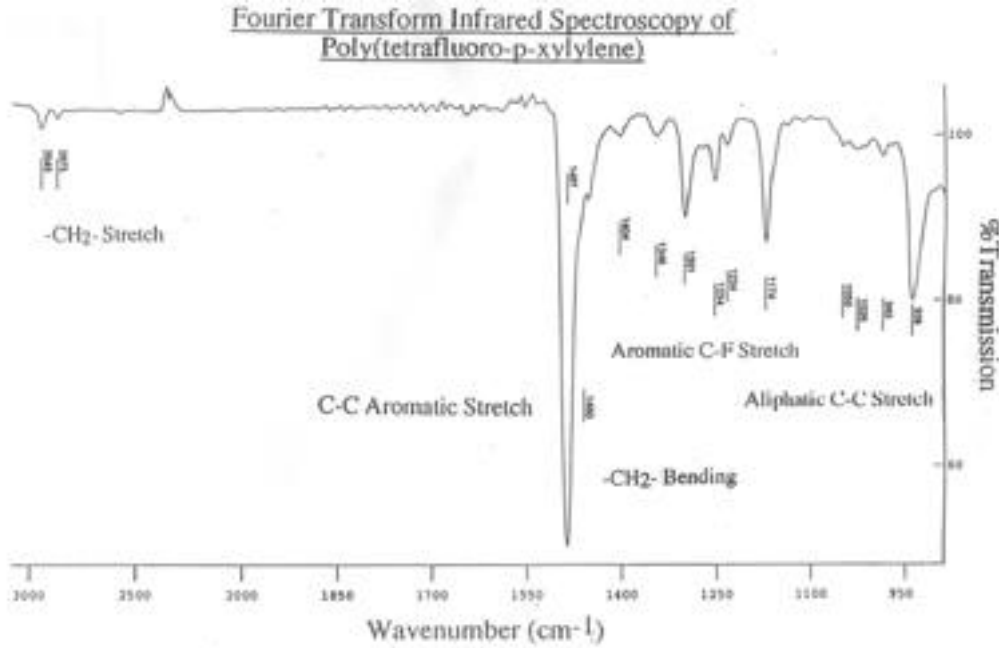

Figure 2 – FTIR spectrum of VT-4

Figures 3 and 4 below show the dispersion of the index of refraction as a function of wavelength for both anisotropic and isotropic models. At 630 nm, the ordinary index of refraction is 1.605 and the extraordinary n is 1.47, which is lower than the n of PPXC (1.66 and 1.63) or PPXN (1.665 and 1.61).[7] This is a result of the lower polarizability of fluorine atoms. The birefringence, defined as $\Delta n = n_{out-of-plane} - n_{in-plane}$, is –0.135 at 630 nm. This large negative birefringence, larger than PPXN (-0.03), PPXC (-0.015), or AF-4 (0.09), indicates that fluorine atoms significantly increase the anisotropic polarizability
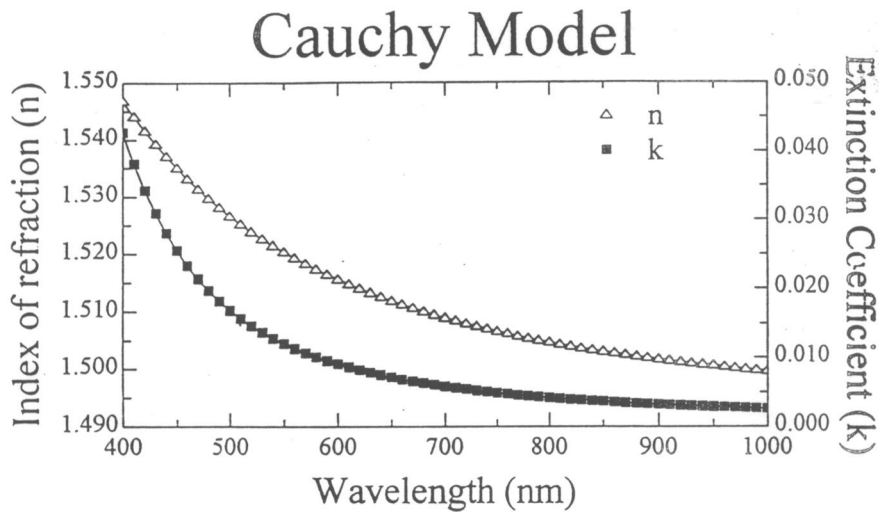
Figure 3 – Isotropic index of refraction for VT-4

38
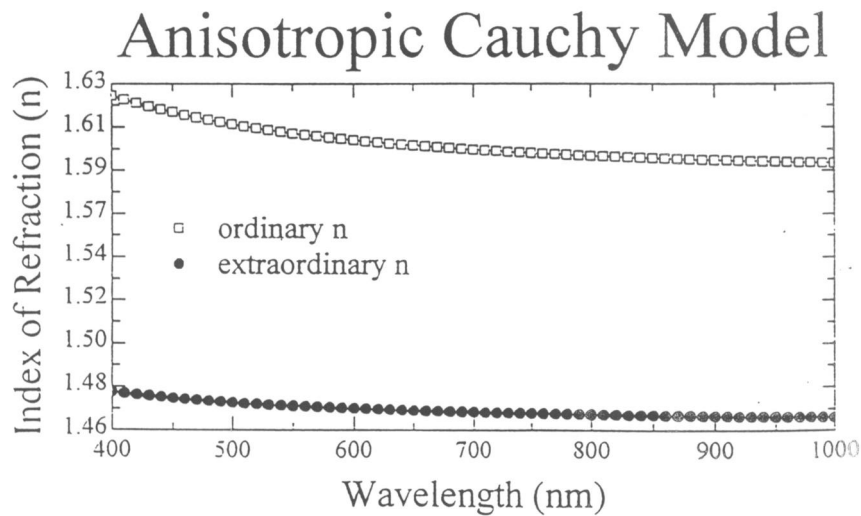
Figure 4 – Anisotropic index of refraction for VT-4

of the benzene constituent of the molecule. While in AF-4, the fluorine atoms are on the alliphatic carbons, the orientation of the benzene ring with respect to the substrate has less effect on the in-plane index of refraction. In VT-4, however, the low extraordinary index of refraction indicates that the benzene rings are aligned in the plane of the substrate, since the in-plane molecular polarizability of benzene is much higher than the out-of-plane polarizability.[8] This has high implications for low-k applications, as a low out-of-plane index of refraction means a low out-of-plane dielectric constant, meaning lower interlayer capacitance effects and thus a lower RC delay.

Table 1 below is a summary of the dielectric properties of VT-4. The dielectric

Frequency	K	Loss
10 kHz	2.50	<0.001
100 kHz	2.46	0.006
1 MHz	2.42	0.008
Leakage Current:	<10e-13 amps	
(tested from 1 to 100V) 15s/1V step, thicknesses 47 and 367 nm		

Table 1 – Dielectric Properties of VT-4

constant can be approximated from the index of refraction at optical frequencies by the formula $k = n^2$. For anisotropic materials, the average index of refraction can be obtained from $n = (n_{out-of-plane} + 2n_{in-plane})/3$, yielding 1.56 for VT-4. Calculating the dielectric constant at optical frequencies yields 2.43, a value very close to that measured at 1 MHz. This is further supported by the low measured loss and the fact that ionic and

orientational polarizability are negligible in the VT-4 molecule. Thus the only contribution to the dielectric constant is electronic polarizability and the dielectric constant will vary little with frequency. The dielectric constant, while not as low as that of AF-4, is lower than any of the other parylenes and thus VT-4 is a promising low-k candidate. Table 2 summarizes the mechanical, electrical and miscellaneous properties of VT-4. The low water absorption is desirable in any semiconductor application, and the thermal expansion information is necessary to ensure compatibility with neighboring adhering materials during thermal cycling. The high modulus and tensile strength are desirable as well, to minimize mechanical failure of the film during processing.

Dielectric Constant	2.3
Dissipation Factor (tanδ)	<0.001
Dielectric Strength (V/cm)	2 x 10^6
Water Absorption (%)	<0.1
Thermal Stability (^{o}C) (<1% wt loss/2 hr)	>450
Volume Resistivity (Ω-cm)	5 x 10^6
Surface Resistivity (Ω)	1 x 10^{14}
Density (g/cm^3)	1.58
Thermal Expansion (ppm@25 ^{o}C)	180
Modulus (Gpa)	2.7
Tensile Strength (MPa)	45

Table 2 – Mechanical and miscellaneous properties of VT-4

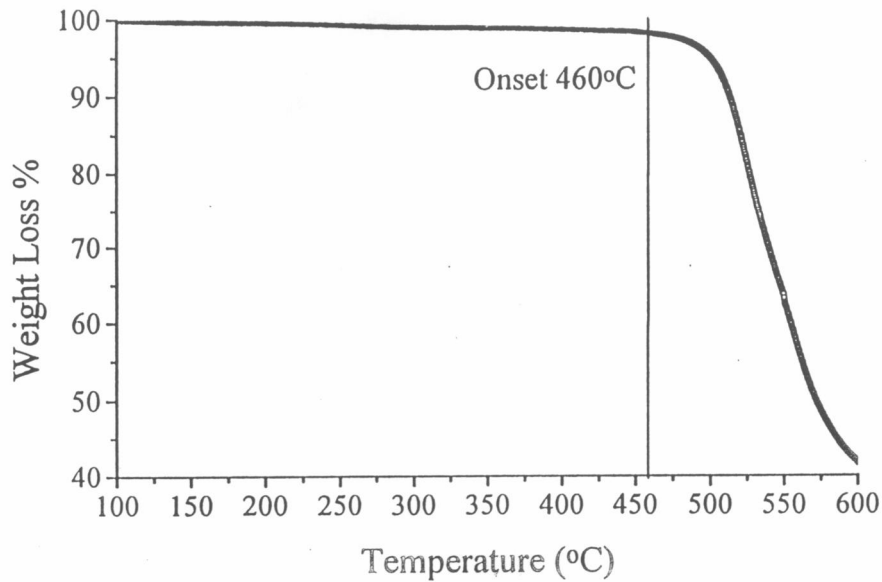Results of the thermal stability analysis are shown in Figure 5. The onset of degradation

Figure 5 – Thermal Stability of VT-4 under Ar atmosphere at 1 ^{o}C/min

occurred at 460 ^{o}C and 1% weight loss occurred at 480 ^{o}C, followed by rapid weight loss. The thermal stability is therefore sufficient to withstand the processing temperatures of 450 ^{o}C used for aluminum metallization. TGA analysis is however not as demanding as the isothermal anneals experienced in the actual processing environment.

VT-4 is a new polymer in the class of parylenes with similar processing requirements. It is a promising candidate for an interlayer dielectric as it satisfies the two major requirements, namely a low dielectric constant (2.42) and thermal stability up to 460 ^{o}C.

REFERENCES

1. A.S. Harrus, M.A. Plano, D.Kumar, J. Kelly, *Mat. Res. Soc. Symp. Proc. Vol.* **443**, 21, (1997).

2. S. Dabral, X. Zhang, X.M. Wu, G.R. Yang, L. You, C.I. Yang, K. Hwang, G. Cuan, *J. Vac. Sci. Tech. B*, **11**, 1825, (1993).

3. L. You, G.R Yang, C.I. Lang, P. Wu, J.A. Moore, *Mat. Res. Soc. Symp. Proc.*, **282**, 593, (1993).

4. W. Groh, A. Zimmerman, *Macromolecules*, **24**, 6660, (1991).

5. W. Beach, C. Lee, D. Bassett, T. Austin, and R. Olson, *Encyclopaedia of Polymer Science and Engineering*, vol. 17, Wiley & Sons, Ny (1984), 990-1024.

6. J.J. Senkevich, S. Desu, *Appl. Phys. Lett.*, **72** (2), 258, (1998).

7. J.F. Gaynor, S. Desu, *J. Mat. Res.*, **11** (1), 236, (1996).

8. J.J. Senkevich, S. Desu, V. Simkovic, to be published in *Polymer*.

9. W.D. Niegisch, *J. Appl. Phys.* **37**, 4041, (1966).

10. S. Kubo, B.J. Wunderlich, *J. Appl. Phys.*, **42**, 4565, (1971).

Chapter 3

Polymer/Siloxane Nanocomposites

ABSTRACT

Polymer/Siloxane nanocomposites were studied as an alternate path to a polymer/silica composite. This study showed that incorporation of a four-ringed liquid siloxane precursor into the parylene PPXC is not feasible. A solid precursor cube-like molecule, vinyl-T8, was incorporated with ease. Pyrolysis of vinyl-T8 at different temperatures revealed complex behavior, with the formation of polymerized vinyl-T8 (through free radical addition at the vinyl groups) as well as silica-like structures forming above $500\,^{\circ}$C as a result of the breaking up of the cage structure of vinyl-T8. Codepositions of PPXC and vinyl-T8 were then examined as a possible path towards a polymer/silica nanocomposite. At deposition temperatures below 5° C, precipitation of excess vinyl-T8 into cubic micron-sized crystals occurred. As this was undesirable, studies were continued at higher deposition temperatures. A Taguchi orthogonal array was set up to study the effect of the sublimation temperatures of the two precursors as well as the pyrolysis temperature and the substrate temperature on the deposition rate, the index of refraction and the weight loss after a $500\,^{\circ}$C anneal. The deposition rate depended mostly on the sublimation temperature of the PPXC and the substrate temperature. The lowest index of refraction (and thus the lowest dielectric constant) was obtained with the lowest sublimation temperatures of $134\,^{\circ}$C for PPXC and 195° C for vinyl-T8 and a pyrolysis temperature of $200\,^{\circ}$C. Each of the factors was found to have an effect on the index of refraction, with the sublimation temperature of vinyl-T8 having the most influence. The films degraded at $500\,^{\circ}$C, indicating that post-deposition annealing of the films did not lead to a conversion of the vinyl-T8 to a SiO_2-like structure (which would be stable at that temperature). X-ray diffraction spectra of the films revealed peaks which were not present for any of the vinyl-T8 films or characteristic of PPXC. Therefore, some type of interaction between the two components occurred and affected the morphology, most like the formation of a block copolymer. Thus, though polymer/silica films were not attained,

the resulting composites had comparable properties with higher deposition rates and a cleaner process.

Introduction

The current intermetallic dielectric employed in the microelectronics industry is SiO_2, which is deposited with techniques such as chemical vapor deposition or plasma enhanced chemical vapor deposition. A desirable replacement with a lower dielectric constant will most easily incorporate in-situ processing technology. Combining the SiO_2 phase with an organic phase with a lower dielectric constant is an attractive option for solving the RC delay problem.[1] Such a process takes advantage of the well understood SiO_2 deposition technology, and does not neutralize the desirable properties of SiO_2 films, such as mechanical strength, thermal stability, thermal conductivity, and high adhesion strength. Furthermore, undesirable characteristics of low-k polymer films such as poor resistance to metal diffusion and a large undesirable dielectric anisotropy can be overcome by combining the organic phase with an inorganic phase. The presence of the SiO_2 phase disrupts the crystallinity of the polymer, thus reducing the anisotropy, leading to a lower in-plane capacitance. PPXC/SiO_2 nanocomposite films were successfully deposited and characterized to achieve this goal.[2] In this process, precursors were converted to vapor phase and pyrolyzed separately, the two phases mixing right before deposition. This led to a phase-separated composite with domains on the nanoscale. The relative phase concentrations could be controlled by adjusting the vaporization temperature of the inorganic phase precursor. This ability to control the phase composition leads to control of the index of refraction as well as the dielectric constant. Thus, in addition to low-k applications, this process could find use in the manufacture of graded index films, waveguides, and antireflection coatings.[3]

Once the SiO_2 precursor di-acetoxy-di-t-butoxysilane decomposes in the furnace, several reactive species are formed. The exact chemistry is not well understood, though attempts have been made to explain it.[4] This decomposition occurs at 650 ^{o}C, and once decomposition of the DADBS molecules occurs, deposition of SiO_2 occurs at any temperature. This is not the case with the polymer case, as PPXC does not deposit above 90 ^{o}C. The optimum temperature of the tubing leading from the point of mixing of the two phases and into the deposition chamber, as well as the deposition chamber walls was

found to be 250 $^{\circ}$C and 110 $^{\circ}$C, respectively. Since PPXC deposits through a condensation process, raising the temperatures any higher than this led to too much kinetic energy being imparted to the gaseous diradical PPXC reactant, and no deposition of the organic phase would occur.

However, at these temperatures, there was significant deposition of SiO_2 all along the delivery path from the pyrolysis furnace to the substrate, creating two undesirable conditions. The concentration of the silica reactants decreased exponentially along the path to the substrate, yielding lower deposition rates than could be achieved with no deposition along the path. Worse yet, the problem increased with each deposition, as the deposited SiO_2 created a rough surface along the inner walls of the reactor tubes, leading to an ever increasing surface area on which the silica could form. Eventually, no reactant would reach the substrate, as it would react to form a film on the surface area available along the way. This necessitated a cleaning of the reactor, a time consuming process, since SiO_2 is a very hard substance with excellent adhesion to metal surfaces. It was the need to overcome these issues that motivated the search for an alternative method of obtaining a silica phase in the nanocomposites. Siloxane molecules that do not readily form SiO_2 upon deposition were studied, effectively eliminating the pyrolysis step. It was hypothesized that upon post-deposition thermal annealing of the nanocomposite films, the inorganic phase would result in SiO_2 or a cross-linked polysilsesquioxane (general formula $RSiO_{3/2}$) structure.

TM-TVCS

The first new precursor studied for the purpose of obtaining an inorganic phase consisting of cross-linked siloxane chains was 2,4,6,8-Tetramethyl-2,4,6,8-tetravinylcyclotetrasilane (TM-TVCS) purchased from Lancaster. The chemical structure of this molecule is shown below in Figure 1. This precursor is a liquid with a boiling point of 110 $^{\circ}$C/10 mm. Nanocomposites of PPXC and TM-TVCS were deposited, varying the vaporization temperature of TM-TVCS to determine the effect on the deposition rates. After determining the optimum vaporization rate, the films were characterized to determine the

incorporation of TM-TVCS into the PPXC film. The films were deposited with a sublimation temperature of 136 ^{o}C for PPXC, a vaporization temperature of 75 ^{o}C for TM-TVCS, pyrolysis temperature of 600 ^{o}C, cross, tubing and deposition chamber walls temperature of 100 ^{o}C, and substrate temperature of 27.5 ^{o}C. The system pressure was around 40 mTorr. Auger electron analysis was used to detect the presence of silicon atoms within the films. FTIR spectroscopy was used to determine the chemical structure of the films. Thermal stability of the films was measured by a series of thermal anneals in both a nitrogen and an oxygen atmosphere.
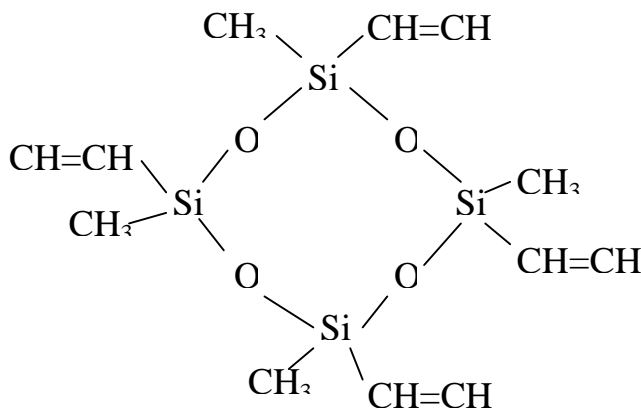
Figure 1 – Chemical structure of TM-TVCS

Results & Discussion

Figures 2 and 3 below show the effect of the vaporization temperature on the deposition rates for two different sublimation temperatures of PPXC. For both sublimation temperatures, the highest deposition rates occurred at vaporization temperatures of 75 ^{o}C. This was chosen as the optimum vaporization rate for TM-TVCS.
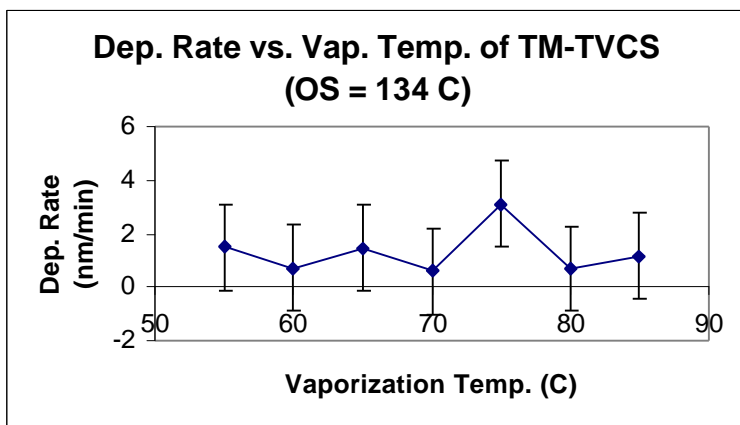
Figure 2
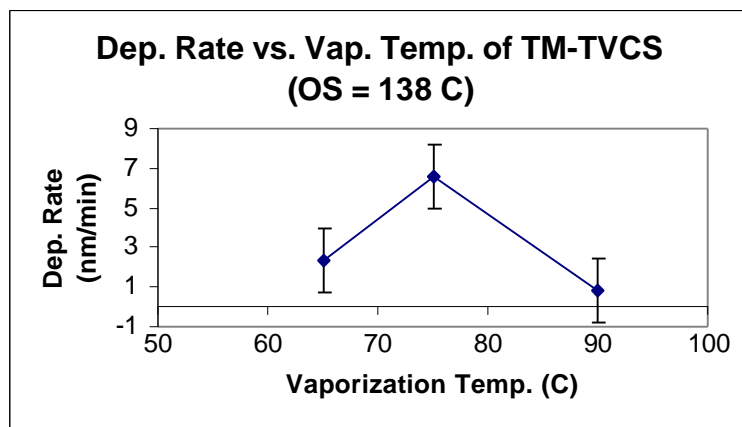
Figure 3

The increase in deposition rate with an increase in the vaporization temperature indicates that some incorporation of the siloxane does take place. The TM-TVCS has a much higher vapor pressure than the dimer precursor of PPXC, and furthermore the diradical formed is much more reactive and adheres to the substrate much faster than the siloxane. The deposition rates drop off for $T_{Vap}>75\ ^oC$, since at 75 ^oC the concentration of TM-TVCS in the gas phase leads to maximum incorporation and any increase in the
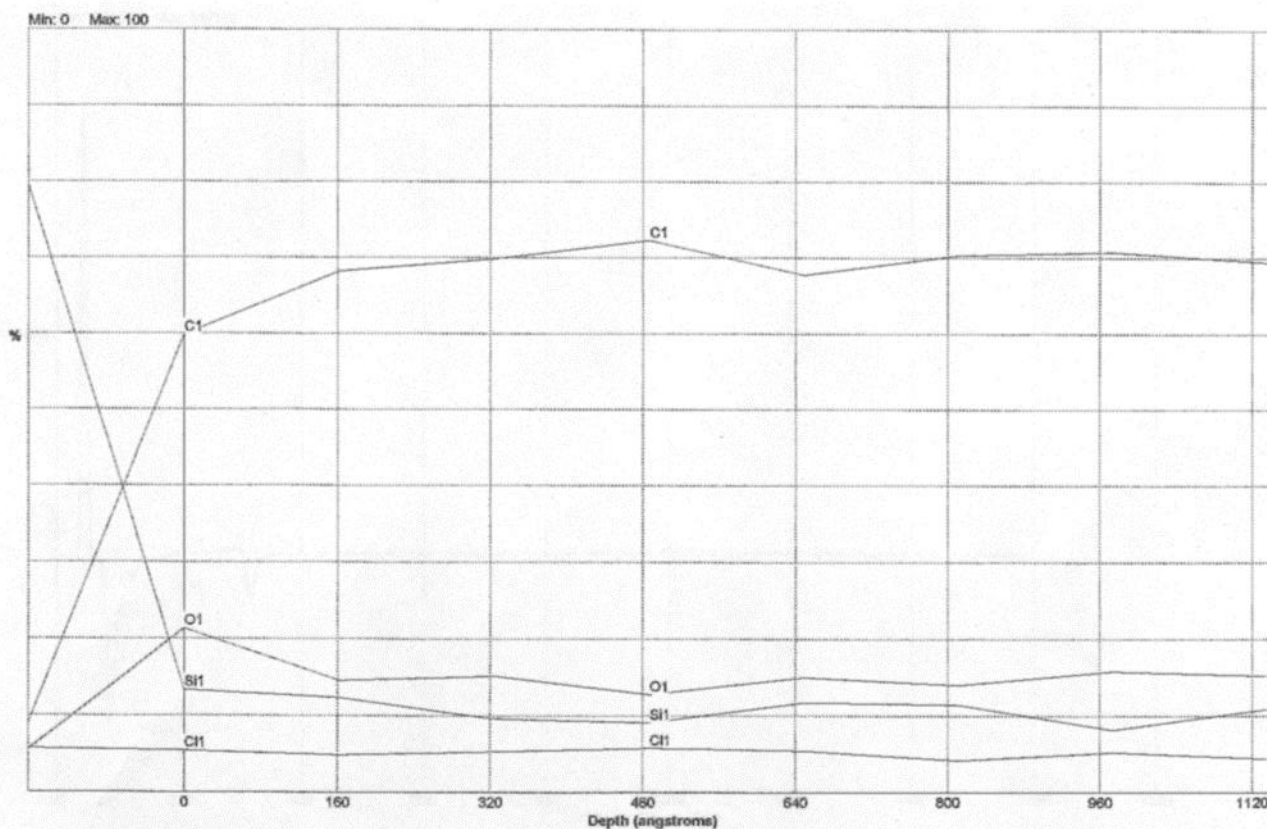
Figure 4 - Auger electron spectroscopy for the as-deposited sample

concentration leads to interference with the diradical species, decreasing the frequency with which they strike the surface. Thus, the incorporation of the TM-TVCS is surface controlled and there is an inherent limit to the process determined by the rate of condensation of TM-TVCS on PPXC and the rate of diffusion of TM-TVCS into PPXC. Results for Auger electron analysis are shown below for both an as-deposited sample and an annealed sample. It can be seen that for the as-deposited sample, the silicon content was about 10%, while the oxygen content was about 15%. Since there is one Cl atom per repeat unit of PPXC, and 4 atoms of Si in one molecule of TM-TVCS, the ratio of PPXC mers to siloxane molecules is 2:1. The extra oxygen is a result of water contamination. This analysis, however, tells us nothing about the relative phase concentrations, as the densities and morphologies of the phases is not known.
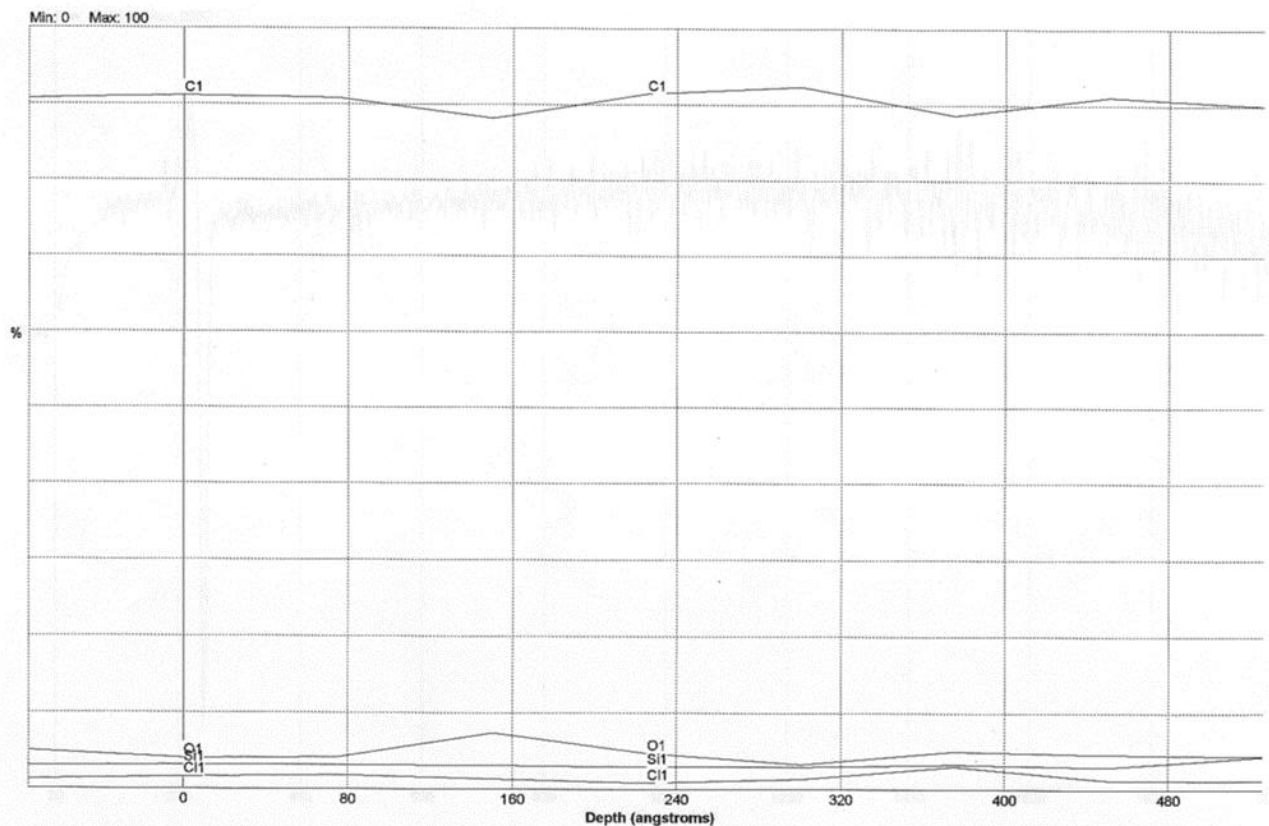
Figure 5 - Auger electron spectroscopy for the annealed sample

The annealed sample underwent a thermal treatment at 450 ^{o}C for 30 minutes under a N$_2$ atmosphere. Most of the Si and O is no longer present, indicating that the siloxane did not bond with the polymer phase and simply evaporated from the film. Figure 6 shown the FTIR spectrum of a PPXC film, while Figure 7 shows the spectrum of a PPXC/TM-TVCS film. Were significant TM-TVCS present, a prominent Si-O-Si peak would be present at 1070-1100 cm^{-1}. Since no such peak is present and the two spectra are nearly
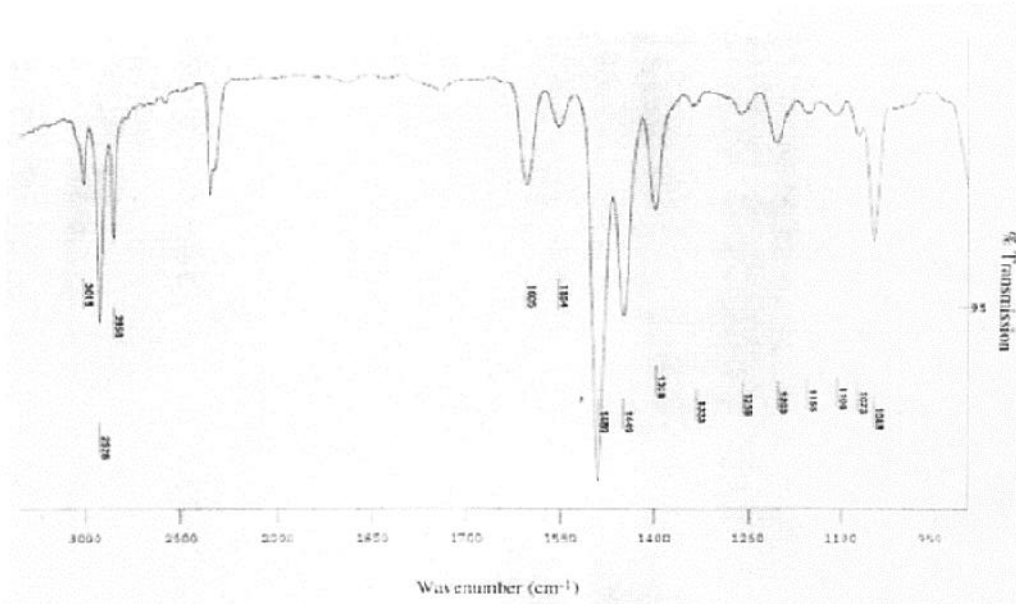
Figure 6 – FTIR spectrum of PPXC
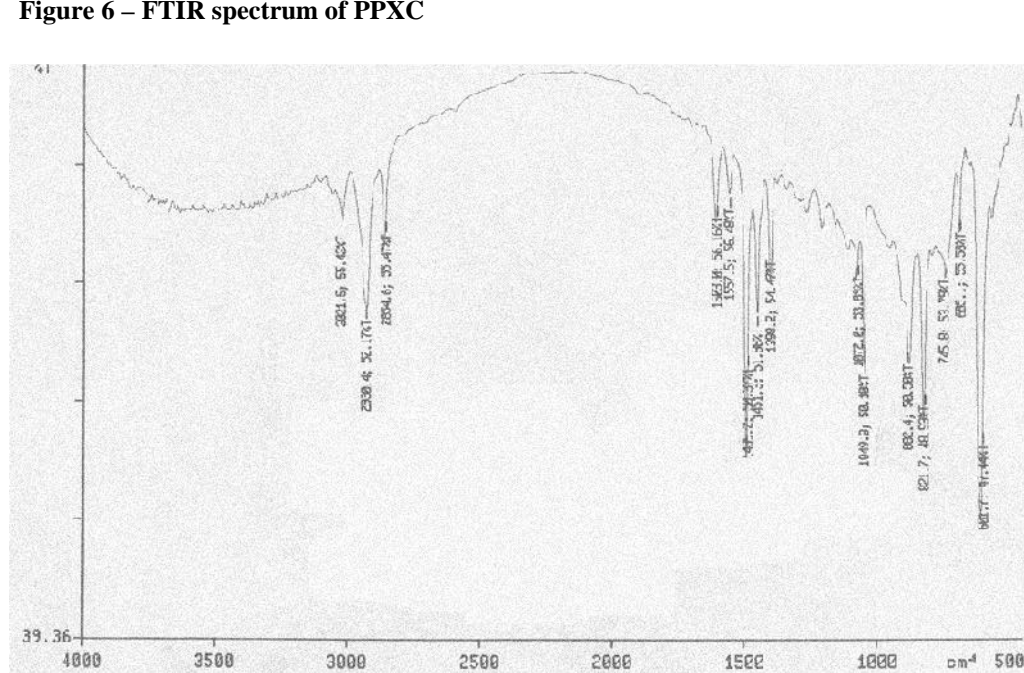
Figure 7 – FTIR spectrum of PPXC/TM-TVCS composite

identical, it must be concluded that the amount of the siloxane incorporated is not significant. The group of peaks at 3015, 2926, 2858 cm^{-1} is a result of C-H stretching corresponding to the three types of C-H bonding that occurs in the PPXC molecule. The
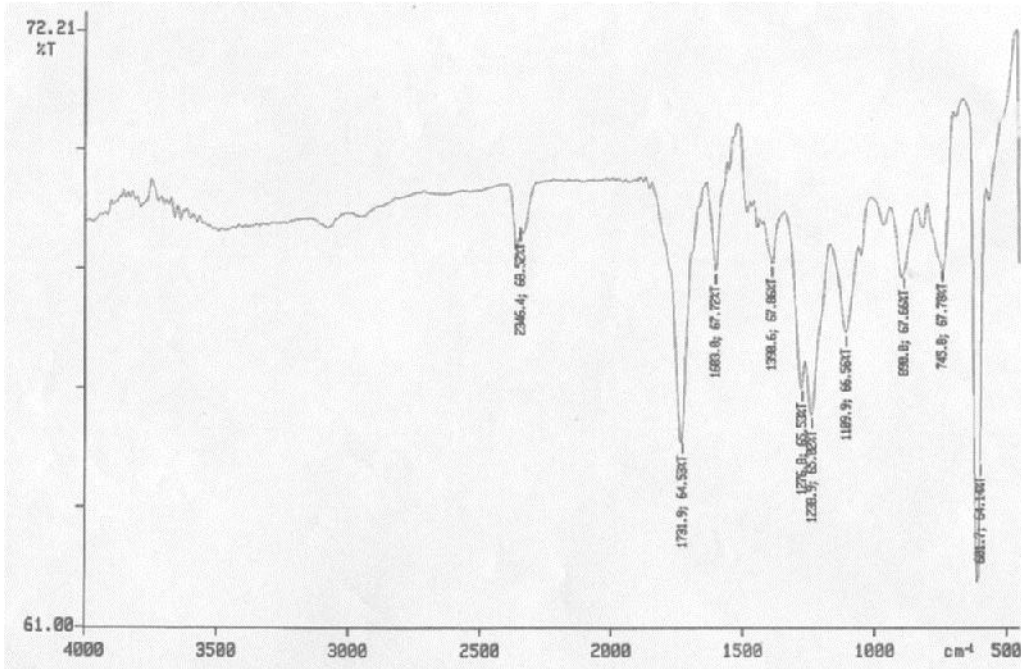

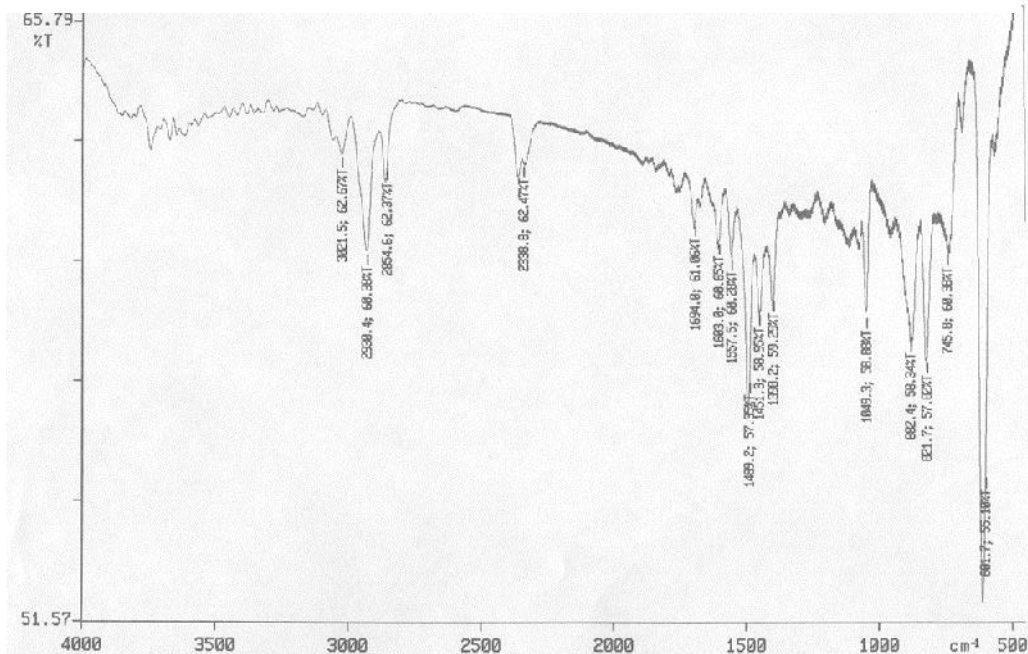**Figure 8 - – FTIR spectrum of PPXC/TM-TVCS composite annealed in O$_2$ at 300 ^{o}C**

Figure 9 – FTIR spectrum of PPXC/TM-TVCS composite annealed in N$_2$ for 400 ^{o}C

1489, 1449, and 1398 cm^{-1} group corresponds to C-H bending in the π-bonding structure as well as the alliphatic C-C bend. The peak at 1605 cm^{-1} is due to aromatic C-C stretching.[5] FTIR spectra of composite samples annealed in both nitrogen and oxygen are shown in Figures 8 and 9. The sample annealed in nitrogen underwent very little change in the chemical bonds present. The sample annealed in oxygen, however, shows extraneous peaks around 1731, 1390, 1276, and 1238 cm^{-1}, which are probably due to the formation of carboxylic acid dimers caused by oxygen degradation. At 300 $^{\circ}$C, PPXC films are ordinarily completely degraded in oxygen and thus the presence of the TM-TVCS somehow improves the thermal stability of the films. A thermal degradation study was performed in both nitrogen and oxygen to determine the stability of the films. Both the thickness and index of refraction were measured with variable angle spectroscopic ellipsometry using angles of incidence of 60°, 65°, and 70°. Modeling was done with anisotropic and isotropic Cauchy models.   Figure 10 shows the decrease in thickness as a function of temperature for both nitrogen and oxygen annealing. Figure 11 shows the
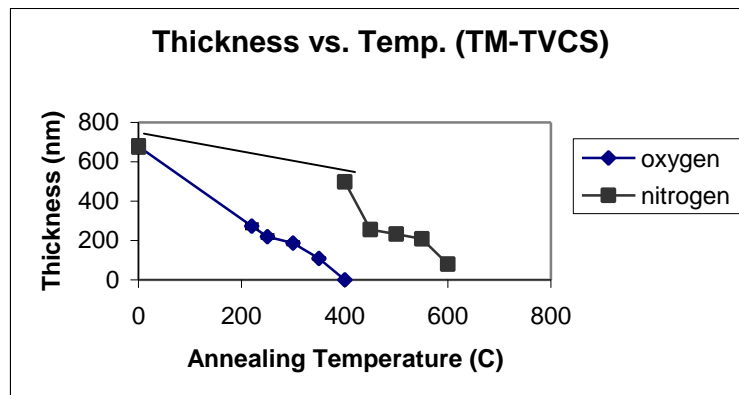

Figure 10

change in the index of refraction as a function of annealing temperature. Both figures show the results of successive 30 minute anneals done on the same sample. In oxygen, there is a steady linear decrease in thickness until the film is gone, indicating that degradation occurs at the same rate from the onset. In nitrogen, the thickness decreases slowly until 400 $^{\circ}$C, at which point there is a sharp drop in thickness, followed by another gradual decrease. The sharp drop represents the onset of degradation of PPXC.   There is no change in the index of refraction in the sample annealed in oxygen, as n remains around 1.66, the index of refraction of PPXC. The sample retained its optical anisotropy,
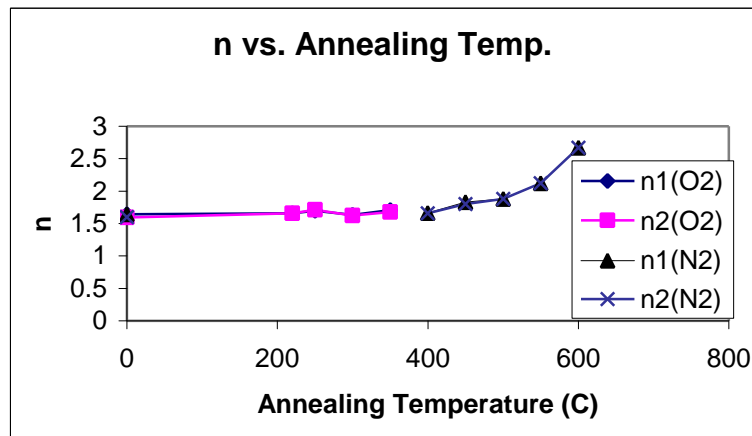
n vs. Annealing Temp.

Figure 11

with a birefringence between -.0176 and .0284. The sample annealed in oxygen underwent an increase in n from 1.66 to 2.67 after the 550 $^{\circ}$C anneal. Optical anisotropy disappeared after the 500 $^{\circ}$C anneal.

In oxygen, film degradation occurs steadily with no evidence of any chemical or morphological changes. Degradation occurs by chain fission at sites of the alliphatic carbons, and the index of refraction does not change as a result of this process.

VINYL-T8

After it was concluded that TM-TVCS incorporates rather poorly into the polymeric film, a siloxane that would eliminate this problem was sought. The lack of incorporation resulted from the high vapor pressure of the liquid four-ringed siloxane. The new siloxane precursor chosen for investigation was 1,3,5,7,9,11,13,15-octavinylpentacyclo-octasiloxane (vinyl-T8). Vinyl-T8 is a solid with a vapor pressure curve shown in Figure 12. The curve is based on the equation Log P = -5500/T+11.63+-2.1, which was obtained empirically in previous literature.[7] The molecular structure of
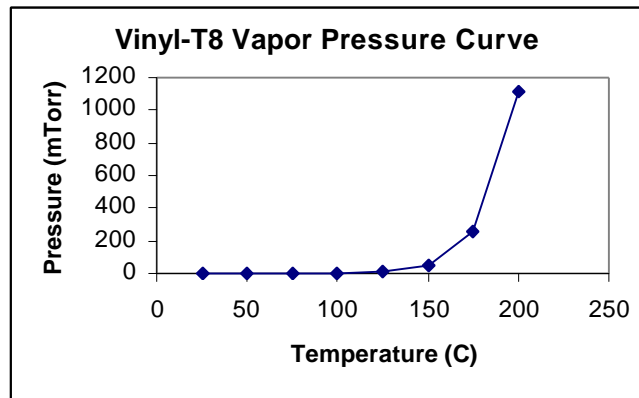

Figure 12

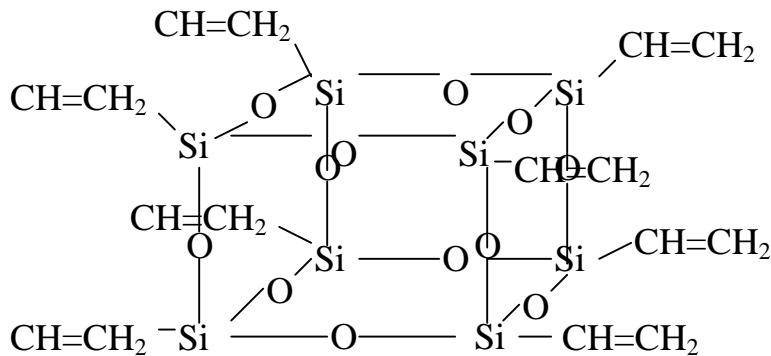vinyl-T8 is shown in Figure 13, which shows a cube-like structure with vinyl groups

Figure 13 – Molecular structure of vinyl-T8

coming off the silicon atoms on the corners. The sublimation temperature of vinyl-T8 was 195 ^{o}C, the pyrolysis temperature was set to 200 ^{o}C, and the substrate and thus deposition temperature was kept at 0-5 ^{o}C. The effect of reactive ion etching on the films was studied by exposing the films to an RF plasma of oxygen at a power level of 10 W, pressure of 600 mTorr, for a time interval of 5 minutes.

Thickness and index of refraction measurements were done using a variable angle spectroscopic ellipsometer and modeling of the data was based on the Cauchy and anisotropic Cauchy models. It has been previously determined that vinyl-T8 dissolves in chloroform, while polymerized vinyl-T8 does not.[7] Therefore, films were dipped in chloroform for one minute to determine the amount of dissolution.

To study the effect of the sublimation temperature of both phases, as well as the deposition temperature and the pyrolysis temperature of vinyl-T8 on the properties of the films, a Taguchi orthogonal array was chosen to design a series of experimental conditions which would yield the maximum information with a minimal number of experiments. Each of the four parameters was studied at three different levels. The array is shown below in Table 2, and the corresponding experimental conditions are shown in Table 3.

Experiment	FACTORS			
	1	2	3	4
1	1	1	1	1
2	1	2	2	2
3	1	3	3	3
4	2	1	2	3
5	2	2	3	2
6	2	3	1	1
7	3	1	3	2
8	3	2	1	3
9	3	3	2	1

Table 2 – Taguchi orthogonal array of factors and levels

Here, OS is the organic sublimation temperature (PPXC), IS is the inorganic sublimation temperature (vinyl-T8), IF is the inorganic furnace temperature that controlled the pyrolysis of vinyl-T8, and SH is the substrate holder temperature.

Sample	OS	IS	IF	SH
v2p74a	134	195	200	15
v2p74b	134	205	400	25
v2p75a	134	215	600	35
v2p75b	137	195	400	35
v2p76a	137	205	600	25
v2p76b	137	215	200	15
v2p76c	140	195	600	25
v2p76d	140	205	200	35
v2p77a	140	215	400	15

Table 3 – Deposition conditions for each experiment

Results & Discussion

Table 4 below shows the results of the pyrolysis temperature study. The mean square
errors of the model fit from the ellipsometry data for some of the films are rather high,
due to the roughness of the films. Therefore there is considerable uncertainty

| Pyrolysis Temp. (C)	N	N after plasma etch	% weight Loss	Dep. Rate (nm/min)	CH3Cl Test	MSE Before etch	MSE after etch
200	1.48	1.75	24	5.3	Mostly dissolved	92	56
300	1.31	1.27	35	16.3	Slightly dissolved	65	68
400	1.29				did not dissolve	54	
500	1.38	1.35	22	4.1	Mostly dissolved	55	41
600	1.47	1.44	1	36.3	Slightly dissolved	95	72
700	1.49	1.31	5	45.4	Slightly dissolved	96	60

Table 4 – Results of the pyrolysis study

in the results that must be taken into account. Samples with a pyrolysis temperature of
400 ^{o}C could not be modeled after the plasma etch due to excessive film roughness and
porosity, which was apparent from the cloudy and rough appearance of the surface of the
films. The index of refraction values are comparable to the n of SiO_2, which is 1.43. The
values are higher than SiO_2 due to the presence of the vinyl groups, which possess easily
polarizable π electrons, though the values are most likely low due to porosity of the films.

Polymerization of vinyl-T8 eliminates the double bond, therefore leading to a lower index of refraction. This is why the n values for plasma etched samples are lower, as reactive ion etching leads to polymerization. The deposition rates for pyrolysis temperature of 600 and 700 ^oC increase significantly, and the thickness losses due to plasma etching drop greatly. Films deposited with pyrolysis temperatures of 200 and 500 ^oC dissolved in chloroform easily, while at other temperatures, this as not the case. Figures 14 - 16 show the x-ray diffractometer spectra and the FTIR spectra for all the samples. The FTIR spectra of the samples are quite similar. This is not surprising, as the infrared spectra of quartz and amorphous silica are very similar, even though the two substances have very different long range orders. This suggests that FTIR spectra yield information only about short range order dominated by the Si-O bond, which does not significantly change as a result of morphology.[8] There are peaks at 3060 and 2958 cm^{-1}, which correspond to symmetric CH_2 stretches. The prominent peaks at 1697 cm^{-1} and at 1409 cm^{-1} are most likely the result of reactions with traces of oxygen or water present in the reactor during deposition, resulting in either C=O bonds or the formation carboxylic acid end groups. The peaks at 1488, 1001, and 967 indicate the presence of the Si-CH=CH_2 group. The fact that these peaks are present at all temperatures indicates that any reactions involving the vinyl group do not reach complete conversion. The large dominant peak which occurs at 1103-1125 is the asymmetric Si-O-Si stretch, while the peak at 774-780 cm^{-1} is the symmetric Si-O-Si stretch.[9,10] This peak has been deconvolved into two or three separate peaks by different researchers for amorphous silica, for which a characteristic asymmetric hump appears near 1150 cm^{-1}.[11,12] The results of the deconvolution suggest that amorphous silica may exhibit a paracrystalline
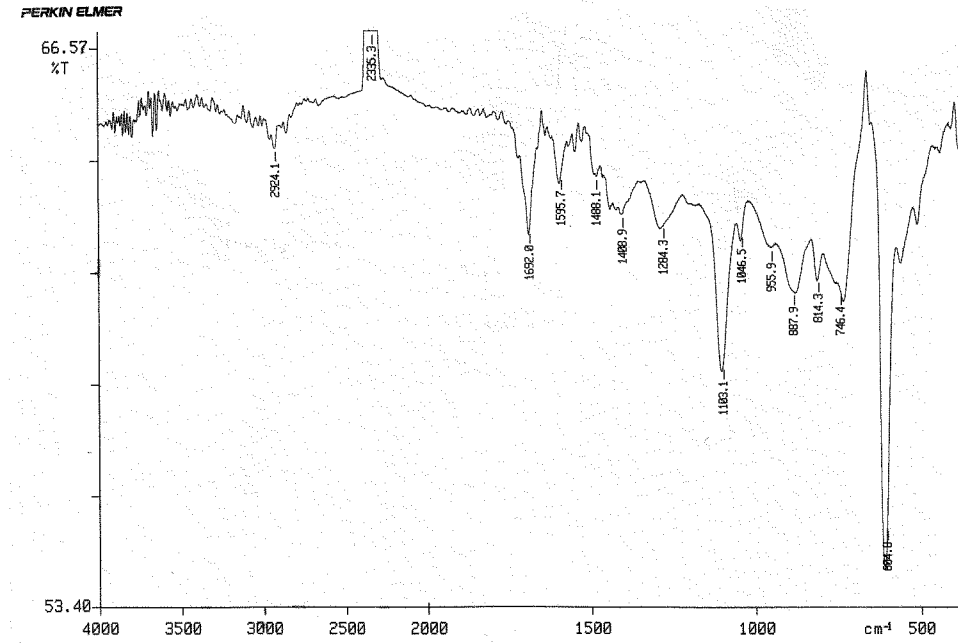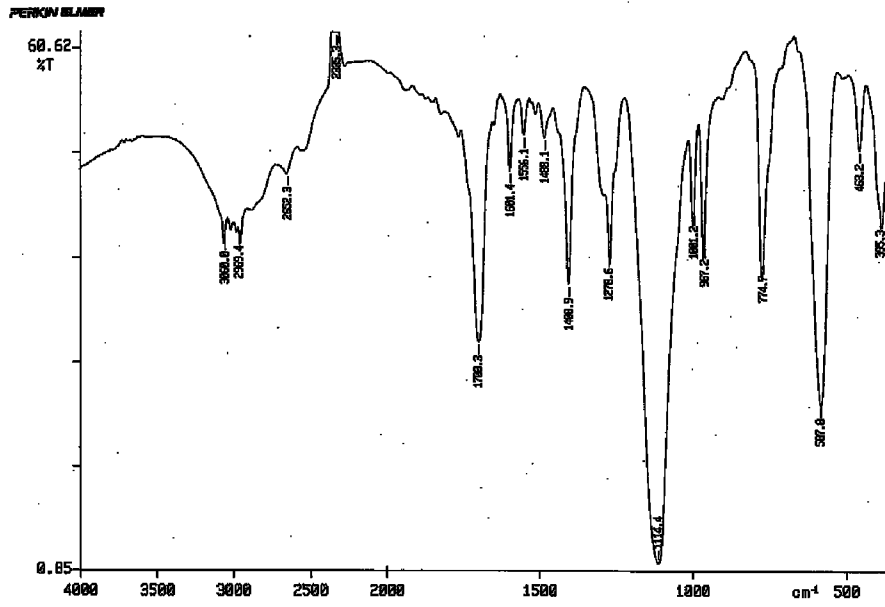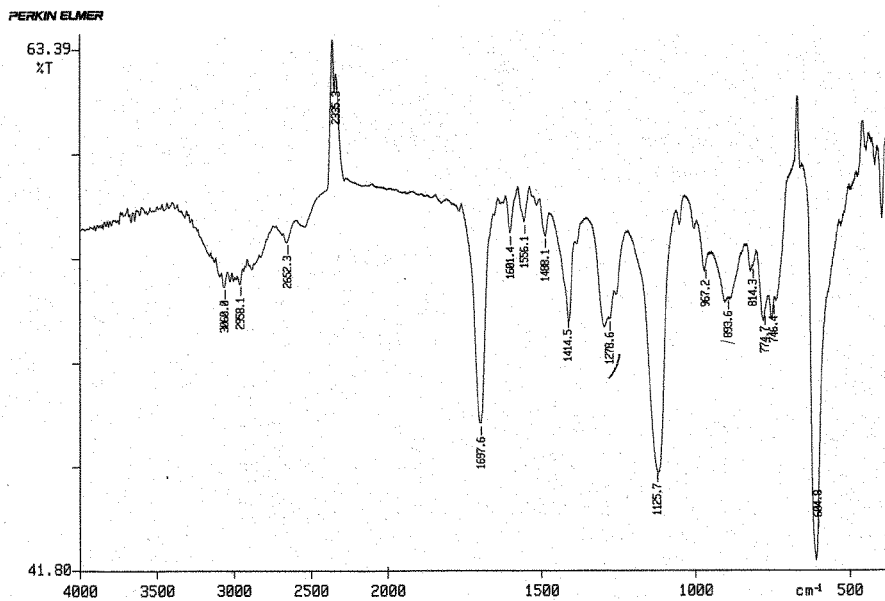
FTIR spectrum of vinyl-T8 for IF = 200 °C
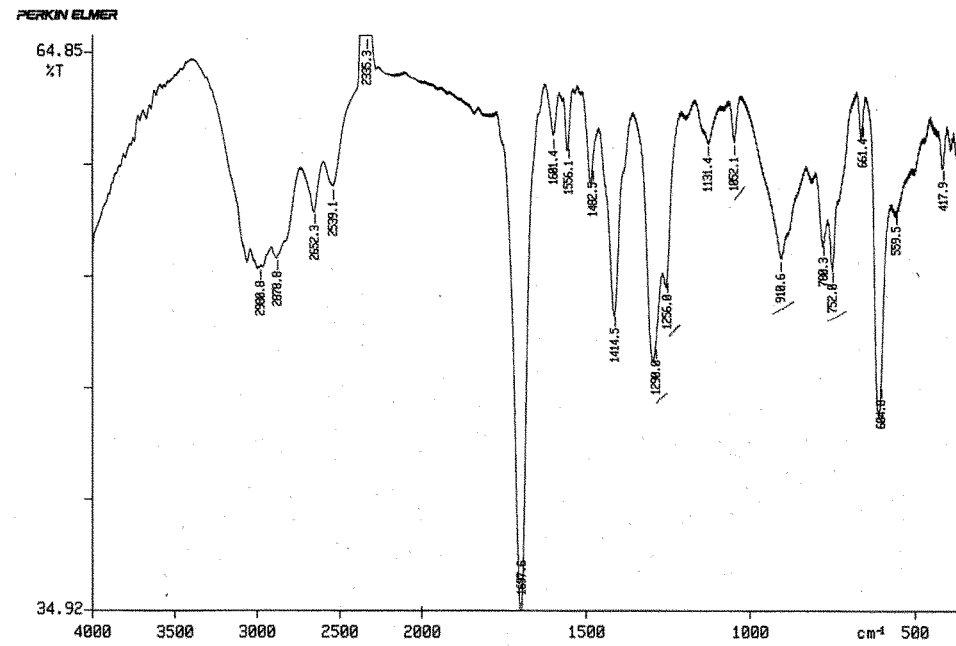
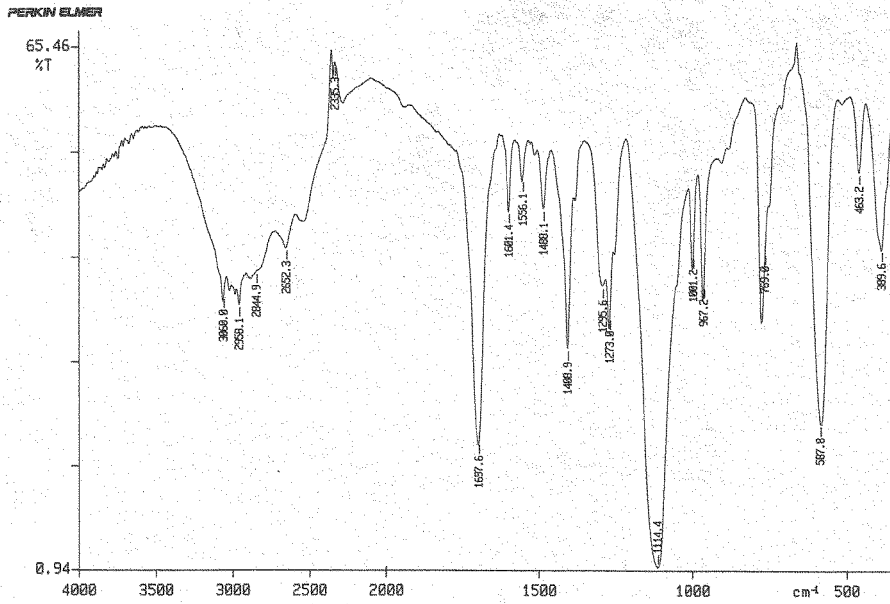

FTIR spectrum of vinyl-T8 for IF = 300 °C

Figure 14

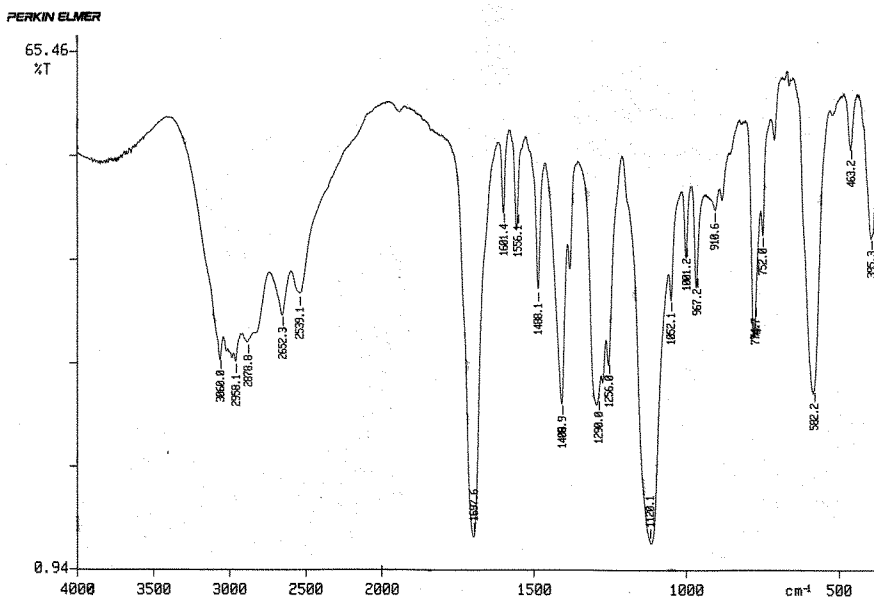FTIR spectrum for vinyl-T8 for IF = 400 °C

FTIR spectrum for vinyl-T8 for IF = 500 °C

Figure 15

FTIR spectrum of vinyl-T8 for IF = 600 °C

FTIR spectrum of vinyl-T8 for IF = 700 °C

Figure 16

structure with nonbridging oxygen atoms present on internal surfaces. As oxide content decreases, the silicon atoms have a higher probability of having a silicon neighbor, which shifts the stretching frequency to higher wavenumbers and eliminating the shoulder.[13,14] That's why the Si-O-Si peak for the vinyl-T8 films exhibits no shoulder and occurs at the higher wavenumbers of 1114-1125 cm^{-1} rather than at 1075 cm^{-1} like for amorphous silica, as the stoichiometry for vinyl-T8 is $SiO_{1.5}$ rather than SiO_2. The FTIR spectra yield the information that some of the original vinyl-T8 is present in films obtained with each deposition temperature. Were SiO_2 form completely at the higher pyrolysis temperatures, this peak would shift to a lower wavenumber and an asymmetric shoulder would appear. Since this does not occur, the formation of amorphous silica or siloxane chains is at best partial.

The XRD results exhibit interesting behavior (Fig 17). A broad diffuse scattering region from 27 to 34 2θ appears for all cases except the 500 ^{o}C case. The peak which appears at 61.5 2θ is due to the (400) reflection of the silicon substrate from the Kβ wavelength.[15] A peak appears at 32.9 2θ for all samples except the 200 and 500 ^{o}C cases. For the 200 ^{o}C sample, the peaks at 25.55 and 28.55 are the (111) plane reflections corresponding to the copper Kα and Kβ radiation wavelengths.[15] Additionally, another broad diffuse region appears for the 200 ^{o}C sample from 11.5-14 2θ, and a sharp peak appears at 58.75 2θ. A peak appears at 30 2θ for the 300 ^{o}C sample, and another peak appears at 23.55 2θ for the 400 ^{o}C sample. No peaks or diffuse regions appear for the 500 ^{o}C sample. There aren't enough peaks to make indexing of vinyl-T8 possible.

Since the two samples which dissolved are the 200 ^{o}C and the 500 ^{o}C, these samples contained mostly vinyl-T8. They are also the only samples that did not contain

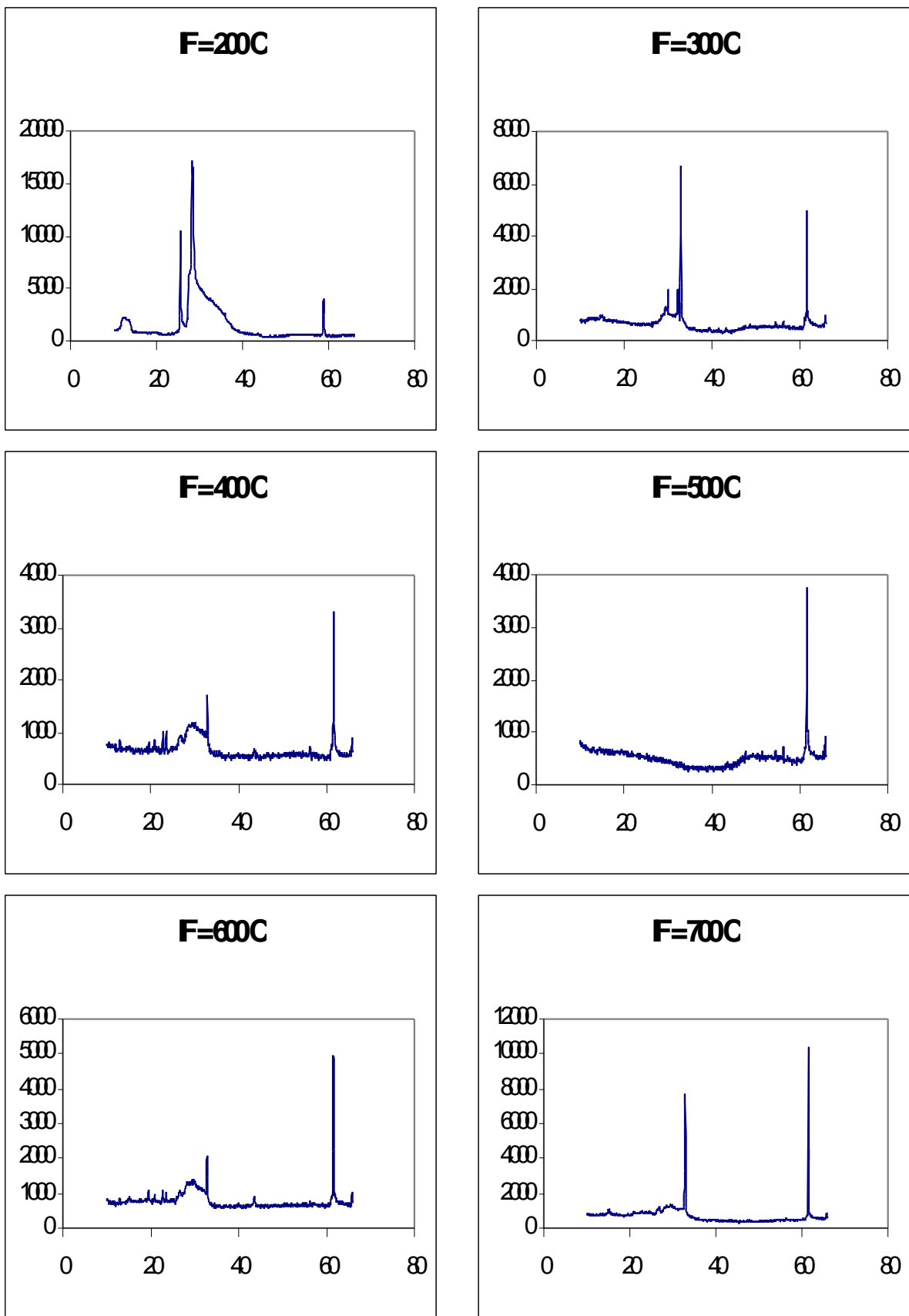**Figure 17 - XRD spectra for vinyl-T8**

the peak at 32.9 2θ. Thus it can be concluded that the vinyl-T8 phase is amorphous.

Samples which did not dissolve in chloroform or dissolved very little contain mostly

polymerized vinyl-T8, which is insoluble. Polymerization has been reported at

temperatures above 200 °C.[16] The polymerized version of vinyl-T8 appears to be

semicrystalline, with the peak occuring at 32.9 2θ corresponding to diffraction from the

crystalline regions. The diffuse halo which occurs for all the samples except the 500 °C

sample is most likely diffuse scattering from regions of intermediate order. Regions of

intermediate order are common in polymeric materials, though models have not been

developed extensively. It has been reported in literature that SiO_2 films can be obtained

from silsesquioxanes such as T8 at temperatures above 500 °C.[17,18] Therefore, the 600

and 700 °C samples consist of a combination of vinyl-T8, polymerized vinyl-T8, and

siloxane chain segments or partial SiO_2 solid networks. The fact that the film structure

approaches SiO_2 can be supported by several facts. Firstly, the Si-O-Si peak for these

two samples is more intense with comparison to the other peaks, indicating the relaitve

predominance of this type of bond in the structure. The considerably faster deposition

rates indicate that the film growth has increased. The partial pressure of the precursor is

the same, thus the surface reactions on the substrate have higher rates. If the cage-like

structure of the vinyl-T8 has been broken, leading to more reaction sites, film growth

would indeed increase. The low loss in weight after plasma etching indicates that the

bonds of the films for these two pyrolysis temperatures are stronger. Si-O-Si bonds are

indeed stronger than carbon to carbon bond of the polymerized form.

However, the formation of SiO_2 is not complete. SiO_2 is amorphous, and yet peaks

appear at 32.9 2θ for both samples. Thus some semicrystalline polymerized vinyl-T8

remains. The peaks which appear for the 300 °C and 400 °C samples at 30 2θ and 23.55

2θ, respectively, might be polymorphic forms of polymerized vinyl-T8, although there is

no evidence to substantiate this. The sample deposited at 500 °C exhibits no features.

Crystallization of the polymeric form does not occur, and there is no indication of

intermediate order. At this temperature, breakdown of the cage-like structure begins to

occur, but not enough reaction sites are formed yet to form a partial SiO_2 network. The

disruption of the T8 cage is enough, however, to prevent any crystallization of the polymeric form.

The pyrolysis temperature chosen for codepositions was 200 ^{o}C, to approximate even distribution of vinyl-T8 within the polymer. To obtain maximum deposition rates and incorporation, initially films were deposited at substrate temperatures of 0-5 ^{o}C. However, as the optical microscopy pictures indicate in Figures 18 – 27, at these deposition temperatures precipitation of the vinyl-T8 phase occurred. Large, micron size cubic crystals appeared in these films. The size of these crystals decreased with increasing deposition temperature, disappearing above 6 ^{o}C. The average crystal size was 42 µm at a deposition temperature of 1.5 ^{o}C, 31 µm at 3.2 ^{o}C, 29 µm at 4.4 ^{o}C, and 10.4 µm at 5.2 ^{o}C. Furthermore, in some films, as in Figure 18, smaller irregularly shaped precipitates could be seen. Dipping a film in chloroform led to dissolution of the crystals, indicating the crystals were vinyl-T8. However, since x-ray diffraction showed the vinyl-T8 to be amorphous, the crystals were polymerized vinyl-T8. Dissolution of the crystals was most likely caused by vinyl-T8 accumulated around the edges, which dissolved, leading to poor adhesion of the crystals to the surrounding substrate, and thus their loosening and elimination from the film, while the film was submersed in solution. The smaller, irregular precipitates were vinyl-T8. FTIR of the films with the crystals removed still showed a Si-O-Si stretching peak at 1119 cm^{-1}, albeit diminished in intensity. Plasma etching at the low power of 20 W led to the opposite effect, shown in Figure 23. The crystals remained behind while the matrix of the film was etched away. This indicates that the polymer in the matrix was of low molecular weight, as this power is too low to cause chain fission. Thus the plasma broke the intermolecular bonds, leading to the degradation of the film. The vinyl-T8 present in the matrix interfered with the polymerization process. Presence of the crystals after etching is further evidence that they are indeed polymerized vinyl-T8, as the intermolecular forces between individual vinyl-T8 molecules would have been disrupted by the ion bombardment from the plasma. Figures 24-27 show the gradual degradation of the film after anneals of 400, 500, 550, and 600 ^{o}C. The anneals were done successively on the same sample for 30 minute intervals under an N$_2$ atmosphere.   It can be seen that the small, irregularly shaped
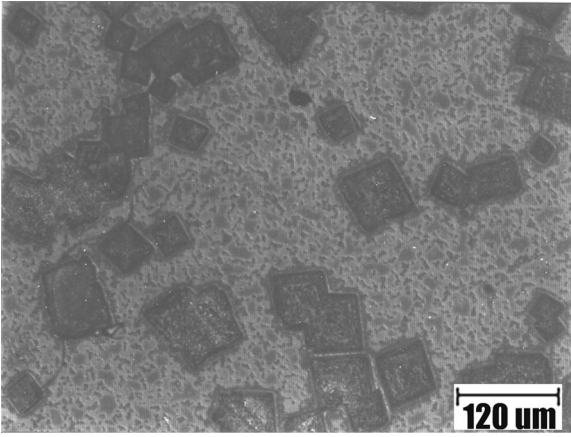
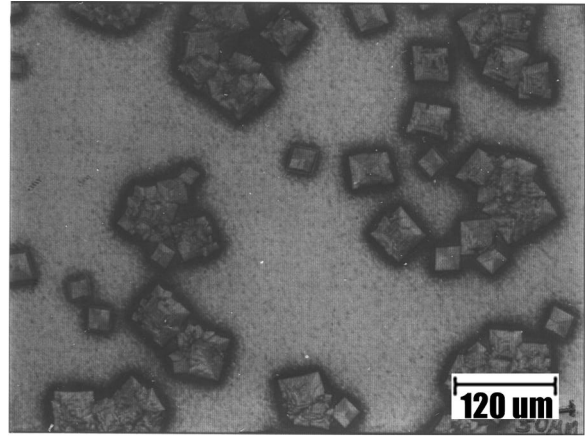**Figure 18 – PPXC/vinyl-T8 film for SH = 1.5 $^{\circ}$C**
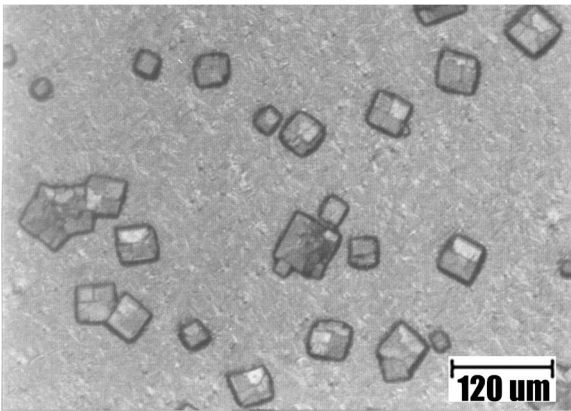

Figure 19 – PPXC/vinyl-T8 film for SH = 3.2 $^{\circ}$C

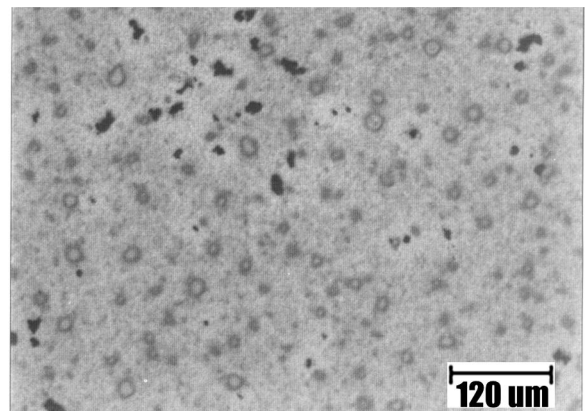**Figure 20 – PPXC/vinyl-T8 film for SH = 4.4 $^{\circ}$C**

Figure 21 – PPXC/vinyl-T8 film for SH = 5.2 $^{\circ}$C
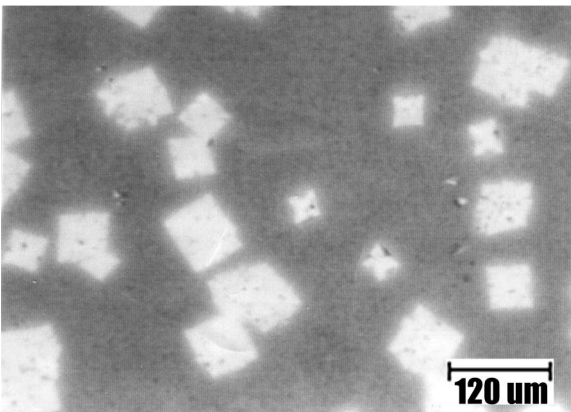

Figure 22 – PPXC/vinyl-T8 film dipped in CH$_3$Cl
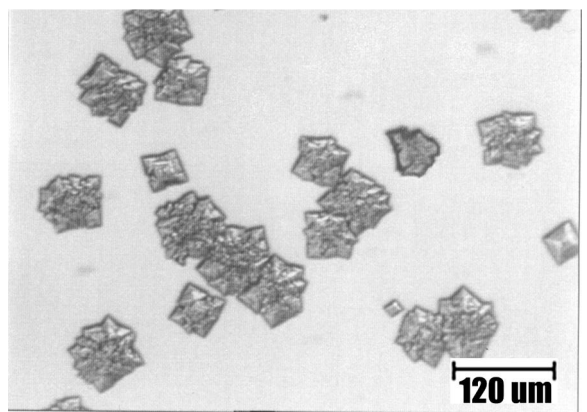

Figure 23 – PPXC/vinyl-T8 after a 20 W/ 3h plasma treatment

65
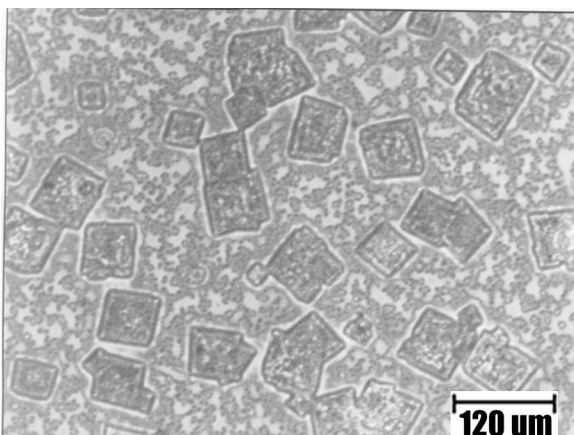
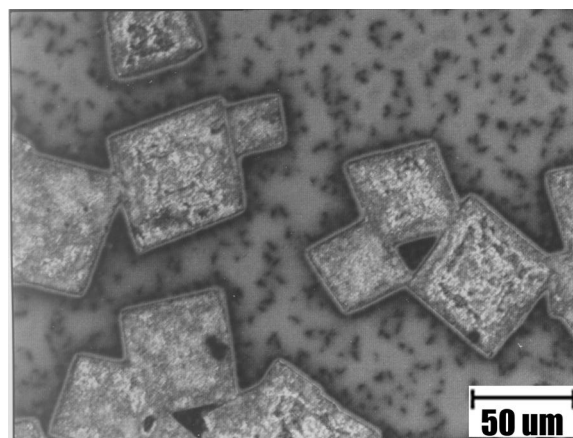**Figure 24 – PPXC/vinyl-T8 film after a 400 $^{\circ}$C anneal**
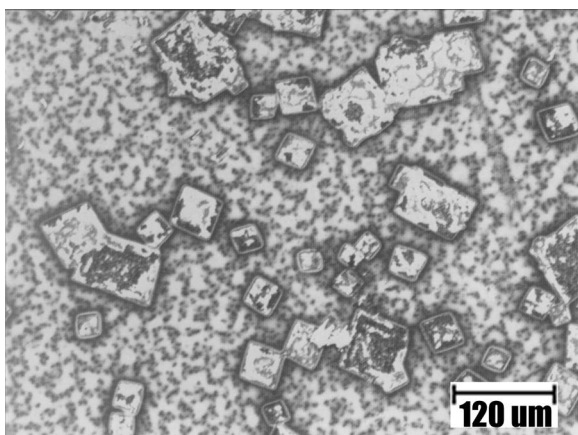

Figure 25 – PPXC/vinyl-T* film after a 500 $^{\circ}$C anneal

Figure 26 – PPXC/vinyl-T8 film after a 550 $^{\circ}$C anneal
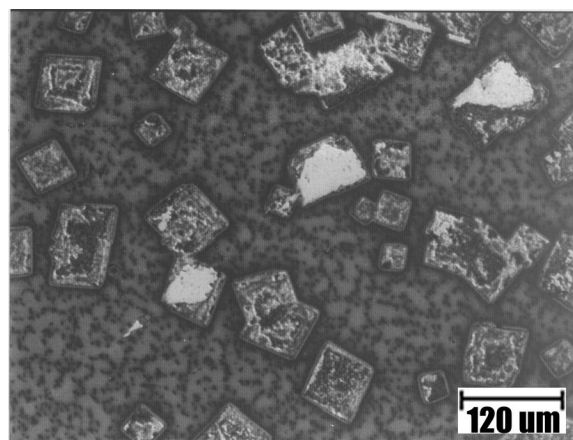

Figure 27 – PPXC/vinyl-T8 film after a 600 $^{\circ}$C anneal

precipitates evaporate after anneals at 500 °C. The polymeric vinyl-T8 crystals begin to degrade at 500 °C as well, a process that continues at 550 and 600 °C. The matrix degrades as well, as can be seen in the reduction of the film thickness as a result of the successive anneals, as shown in Figure 28 below.
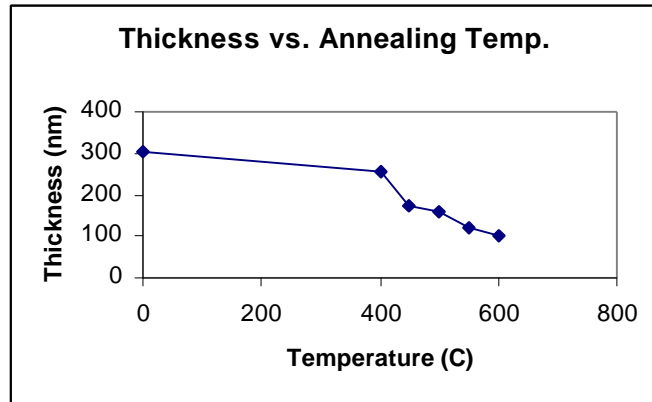

Figure 28

As the formation of the precipitates is undesirable, further studies of PPXC/vinyl-T8 composites were done with the deposition temperatures from 15-35 °C.

The results of the experiments based on the Taguchi array are shown below in Table 5. The thickness and index of refraction measurements and their standard

Sample	Thickness (nm)	St. Dev.	Dep rate (nm/min)	n1	St. Dev.	N2	St. Dev.	SiO$_2$ Peak (cm^{-1})	% weight loss
v2p74a	1387	254	23.1	1.298	0.059	1.296	0.072	1120	100
v2p74b	1711	106	28.5	1.548	0.049	1.523	0.045	1126	97
v2p75a	1044	226	16.1	1.619	0.051	1.662	0.044	1126	92
v2p75b	443	70	7.4	1.393	0.073	1.36	0.093	No	93
v2p76a	455	101	7.2	1.717	0.078	1.679	0.095	1120	49
v2p76b	747	167	12.4	1.800	0.299	1.753	0.271	1126	75
v2p76c	422	100	6.9	1.710	0.067	1.691	0.078	no	53
v2p76d	75		1.2	1.687		1.507		1114	100
V2p77a	269	210	4.5	1.621	0.099	1.565		1126	79

Table 5 – Results of the PPXC/vinyl-T8 study

deviations were calculated from four samples. For the cases where no standard deviation appears, fewer than four samples were available. The fact that the standard deviation for the thickness measurements is high suggest high variancein the deposition rates, indicating that factors other than the four chosen are of importance. The SiO_2 peak of the FTIR spectra appeared for all samples but two. The two samples without the peak were both at the lowest sublimation temperature of vinyl-T8, where not enough vinyl-T8 was sublimed to be incorporated at a high enough rate. ANOVA analysis of these results is presented in the tables below. Table 6 shows the average performance for each factor at each level, for three outcomes of interest: the deposition rate, the index of refraction, and the weight loss after a 30 minute annealing treatment at $500\,^{o}C$ under nitrogen.

OS	Dep. Rate	N	% wt. Loss	IS	Dep. Rate	n	% wt. Loss
134	22.6	1.490	96	195	12.5	1.461	82
137	9.0	1.620	72	205	12.3	1.624	82
140	4.2	1.643	77	215	11	1.673	82
IF	Dep. Rate	N	% wt. Loss	SH	Dep. Rate	n	% wt. Loss
200	12.3	1.570	92	15	13.3	1.561	84
400	13.5	1.508	89	25	14.2	1.649	66
600	10.1	1.681	65	35	8.2	1.547	95

Table 6 – Average performance of each factor

From these results, to maximize the deposition rate, the combination of factor levels should be: OS = 134 ^{o}C, IS = 195 ^{o}C, IF = 400 ^{o}C, SH = 25 ^{o}C. However, the average performance of the sublimation and pyrolysis temperature factors did not vary much over the levels studied, which is confirmed in Table 7 below. It is interesting that the deposition rate decreased with increasing sublimation temperature of the polymer. This contradicts known behavior and common sense, and indicates some interaction between the two precursors in which the two components inhibit each other's growth. It is expected that higher sublimation rates for either component would lead to higher composition of that component in the composite. This is indeed true. Firstly, the SiO_2 peak does not appear at lower sublimation rates of vinyl-T8. Secondly, the index of

refraction increases with increasing sublimation temperature of PPXC, approaching the value of n for PPXC (n=1.65) for OS = 140 ^{o}C. Higher sublimation temperatures for vinyl-T8 lead to an index of refraction which approaches 1.67, again indicating that some interaction between the two components is taking place, as this value is higher than that for either vinyl-T8 or PPXC. This interaction is not desirable, as it leads to higher n values, which mean higher dielectric constants. To obtain the minimum index of refraction and thus the lowest k, one would choose OS = 134 ^{o}C, IS = 195 ^{o}C, IF = 400 ^{o}C, SH = 35 ^{o}C. The weight loss after annealing is a crude estimate of the thermal stability. Degradation occurred at 500 ^{o}C, indicating that conversion of vinyl-T8 to a silica-like network did not occur to a great extent. The highest pyrolysis temperature of 600 ^{o}C yielded the least weight loss, indicating some formation of silica, but not enough to form a continuous network and thus prevent degradation.

Deposition Rate				
Factors	**F**	**S**	**V**	**P**
OS	2	542	271	83%
IS	2	5	3	1%
IF	2	19	10	3%
SH	2	64	32	10%
Error	0	24		4%
Total	8	654		100%

Table 7 – The effect of each factor on the dep. rate

Variance rations could not be computed, because the degrees of freedom for the error term were zero. This could be circumvented by pooling the variance of the error term with the factors which have minimal percent contributions, namely IS and IF.[19] However, this essentially eliminates half of the factors from consideration, thus it was not done.

Tables 7 and 8 show the percent contribution of each factor to the deposition rate and index of refraction. The deposition rate was determined mostly by the sublimation temperature of the polymer and to a lesser extent by the substrate temperature. Contribution to the data spread from other sources was small. The index of refraction

was controlled largely by the sublimation rate and pyrolysis temperature of the vinyl-T8, although the sublimation rate of the polymer and the substrate temperature also had an

| Index of refraction				
Factors	**F**	**S**	**V**	**P**
OS	2	0.025	0.0127	14%
IS	2	0.075	0.0377	42%
IF	2	0.047	0.0236	26%
SH	2	0.020	0.0099	11%
Error	0	0.013		7%
Total	8	0.180		100%

Table 8 – The effect of each factor on the index of refraction

effect. The fact that the deposition temperature affected the index of refraction is interesting. This means that either the incorporation of one of the components was affected by the substrate temperature or that the substrate temperature determined to some extent the interaction of the two components or their resulting morphology.

X-ray diffraction spectra for three different vinyl-T8/PPXC composites are shown below in Figures 29, 30. The first spectrum is for a composite deposited with OS = 134 ^{o}C, IS = 215 ^{o}C, IF = 600 ^{o}C, and SH = 35 ^{o}C, thus this film should have a high vinyl-T8 content and the high pyrolysis temperature indicates the possibility of some silica-like structure. The second spectrum is of the same sample after a plasma etch. Three peaks appear at 19.6^{o}, 29.62^{o}, and 56.38^{o} 2θ (which is most likely the (311) plane reflection from the Kα wavelength for the Si substrate). None of these peaks appeared for any of the vinyl-T8 XRD spectra. Furthermore, the one major peak which appears from 13.80^{o} to 14.30^{o} 2θ for the crystalline phase of PPXC[20] is not present. Therefore, these three peaks indicate the presence of a new crystalline phase, quite possibly a block copolymer of vinyl-T8 and PPXC. Gaynor and Desu have shown that this is what occurs with many comonomers if the vapor pressure of the parylene precursor is maintained low enough.[19] After plasma etching of the sample, as the second spectrum shows, several new peaks
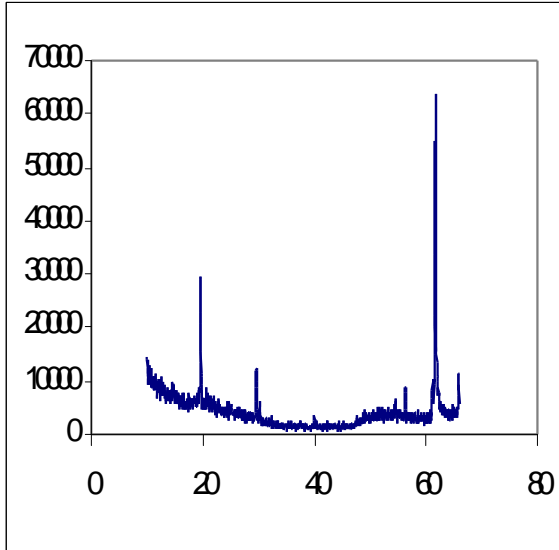
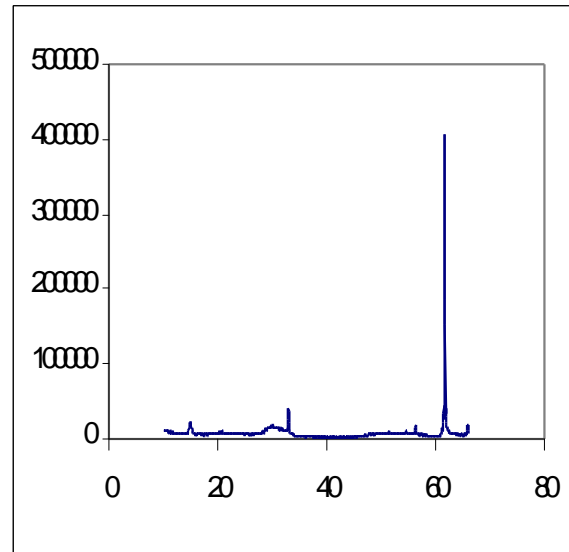XRD for composite film as-deposited
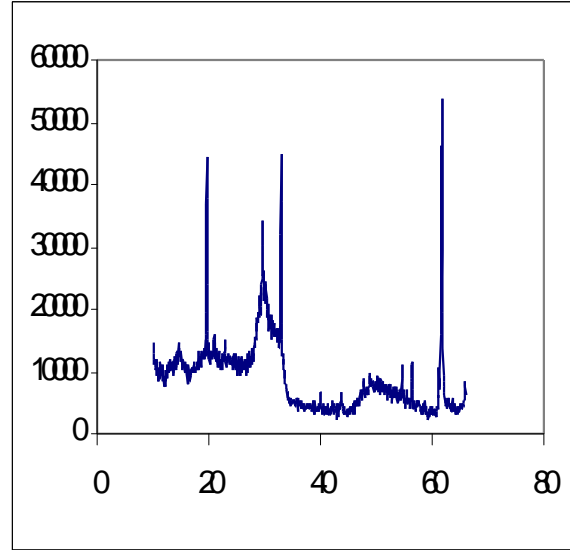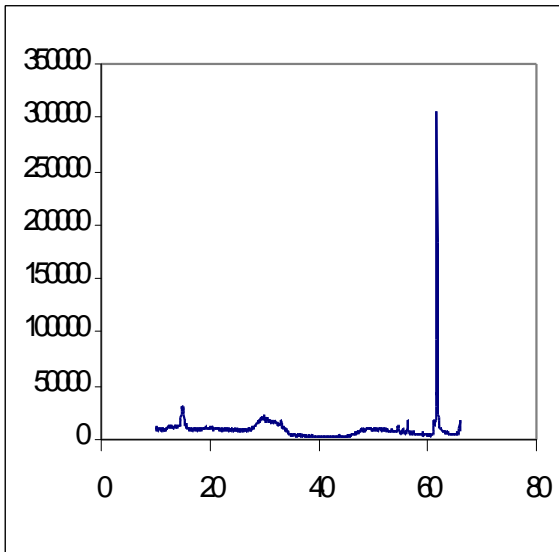
after a plasma etch

OS = 134 ^{o}C, IS = 215 ^{o}C, IF = 600 ^{o}C, and SH = 35 ^{o}C

 XRD for composite film as-deposited

after a plasma etch

OS = 137 ^{o}C, IS = 195 ^{o}C, IF = 400 ^{o}C, SH = 35 ^{o}C
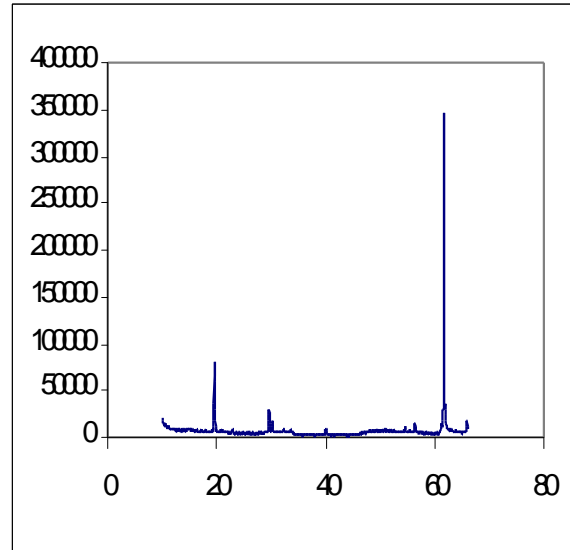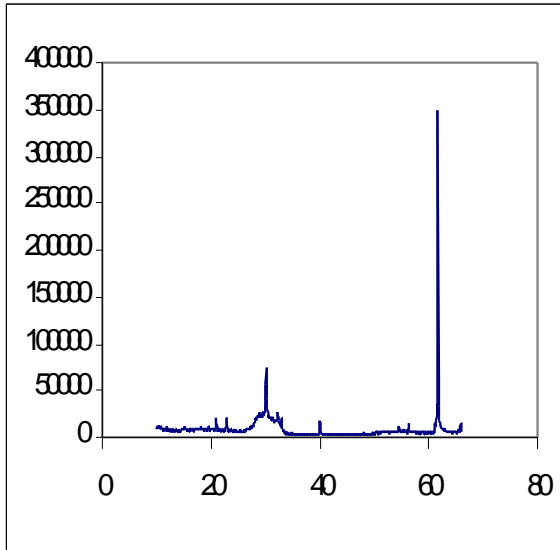
Figure 29

XRD for composite film as-deposited   after a plasma etch

OS = 140 ^{o}C, IS = 205 ^{o}C, IF = 200 ^{o}C, SH = 35 ^{o}C

Figure 30

appear. The broad halo that occurred for all the vinyl-T8 samples from 28.4 to 33.7 2θ
appears, as does the peak which occurred for all vinyl-T8 films pyrolyzed above 300 ^{o}C
at 32.9^{o} 2θ. Additionally, another broad halo appears from 47° to 53.6^{o} 2θ and two peaks
occur at 54.6^{o} and 14.65^{o} 2θ. The plasma treatment therefore resulted in some
polymerization of vinyl-T8 (appearance of the 28.4-33.7^{o} 2θ diffuse region and the 32.9^{o}
2θ peak) and crystallization of PPXC (appearance of the 14.65^{o} 2θ peak). The other
diffuse region that appears and the peak at 54.6^{o} 2θ might be the result of partial
crystallization of the copolymer, although there isn't enough data to substantiate this
claim.

The second set of spectra are of a film as-deposited with OS = 137 ^{o}C, IS = 195 ^{o}C, IF =
400 ^{o}C, and SH = 35° C, and of the film after a plasma etch. This film should therefore
have a higher PPXC content than the previous film. Indeed, a peak at 15° 2θ, though
slightly shifted, indicated the presence of some crystallized PPXC. The broad diffuse
region from 29.5^{o}-34.5^{o} 2θ indicates the presence of some vinyl-T8. After the plasma
etch, the polymerized vinyl-T8 peak appears at 33° 2θ. Thus, in this film, not enough
vinyl-T8 was incorporated for any significant interaction between it and the parylene to
occur.

The third set of spectra are of a film as-deposited with OS = 140 $^\circ$C, IS = 205° C, IF = 200° C, SH = 35°, and of the film after the plasma etch. The as-deposited film does not show the PPXC peak, though the broad region of 28.45-34° 2θ and the peak at 32.3° 2θ indicate the presence of vinyl-T8 and polymerized vinyl-T8. After the plasma etch, this diffuse region and the peak disappear, and two peak appear at 19.6° and 29.65° 2θ. These are the same two peaks which appeared for the first sample and were attributed to a possible crystalline phase of a copolymer of PPXC and vinyl-T8.

The focus of this work, which was the formation of an alternate pathway to a polymer/silica nanocomposite through the use of a siloxane, was not accomplished, as significant formation of silica did not occur through post-deposition annealing. Post-deposition annealing led to film degradation, where a silica phase would be stable at those temperatures. However, polymer/siloxane composites were formed, leading to a copolymer. The properties of these composites were comparable to those containing silica, with an index of refraction ranging from 1.3 to 1.65, depending on the deposition conditions. The advantage of this process is that the siloxane does not deposit on the reactor walls after passing through the pyrolysis chamber, thus leading to a cleaner process with higher deposition rates.

REFERENCES

1. 1. R.D. Miller, J.L. Hedrick, D.Y. Yoon, R.F. Cook, J.P. Hummel, *MRS Bulletin,* **22** (10), p. 44 (1997).

2. J.J. Senkevich, S.Desu, to be published in *Chemistry of Materials*, July 19, 1999.

3. See ref. 2

4. R. Hofman, J.G.F. Westheim, V.A.C. Haanappel, T. Fransen, P.J. Gellings, *Thermochimica Acta*, **215** (1993), p. 329-335.

5. J.J. Senkevich, S.Desu, *Thin Solid Films*, **322**, p. 148 (1998).

6. N.B. Colthup, L.H. Daly, S.E. Wiberly, *Introduction to Infrared and Raman Spectroscopy 3rd ed.*, Academic Press, 1990.

7. V.P. Korchov, T.N. Martynova, V.I. Belyi, *Thin Solid Films*, **101** (1983), p. 373-376.

8. I.W. Boyd, *Appl. Phys. Lett.*, **51** (6), (1987), p. 418-420.

9. See ref. 6.

10. M. Diem, *Introduction to Modern Vibrational Spectroscopy*, John Wiley & Sons: New York, 1993.

11. See ref. 8.

12. A. Goullet, C. Charles, P. Garcia, G. Turban, *J. Appl. Phys.*, **74** (11), (1993), p. 6876-6881.

13. P.G. Pai, S.S. Chao, Y. Takagi, *J. Vac. Sci. Technol. A*, **4** (3), (1986), p. 689-693.

14. R.M. Almeida, C.G. Pantano, *J. Appl. Phys.*, **68** (8), (1990), p. 4225-4231.

15. B.D. Cullity, *Elements of X-ray Diffraction 2nd ed.*, Addison-Wesley: Reading, Mass., 1978.

16. See ref. 7.

17. M.D. Nyman, S.B. Desu, C.H. Peng, *Chem. Mater.*, **5**, (1993), p. 1636-1640.

18. S.B. Desu, C.H. Peng, T. Shi, P.A. Agaskar, *J. Electrochem. Soc.*, **139** (9), (1992), p. 2682-2685.

19. R. Ranjit, *A Primer on the Taguchi Method*, Van Nostrand Reinhold: New York, 1990.

20. J.J. Senkevich, S.Desu, to be published in *Polymer*, 1999.

Chapter 4
Summary

The main contributions of this work were to demonstrate the feasability and analyze the performance of a chemical vapor deposition reactor design capable of processing 8" wafers as well as the characterization of a new parylene polymer and parylene/siloxane composites. The reactor, capable of depositing films with two different precursors with different pyrolysis temperatures, functioned properly. The design was an improvement over an older system, with the most significant improvements being the implementation of a showerhead inlet into the deposition chamber to ensure a more uniform gas flow, and separate heating controls for the walls of the deposition chamber and the substrate holder. A linear pressure vs. flow rate profile ensured a constant pressure gradient between the deposition chamber and the system pump. Thickness measurements along an 8" wafer showed at most a 14% variation in thickness between the minimum and maximum thickness of the film with a higher thickness in the regions of the wafer closer to the showerhead inlet. Films of various parylene polymers, such as PPXN and PPXC, as well as SiO_2 and $PPXC/SiO_2$ composites were deposited with comparable properties and deposition rates. A deposition rate study of PPXC was done to study the effect of the sublimation, pyrolysis, and substrate temperature on the deposition rate. The substrate temperature was shown to have the greatest effect, while the pyrolysis temperature had littlel effect. Large variance in the data showed that other factors are significant. These results demonstrated that scaling of a chemical vapor deposition system does not significantly affect the deposition rates or the film properties. However, the large variance in the deposition rates indicates that the gas flow and kinetics are not simple and are sensitive to other factors besides the sublimation rate and the deposition temperature.

A new polymer in the parylene family, VT-4 was deposited and studied. The main motivation for the development of this polymer was to find a cheaper alternative to AF-4, the fluorinated parylene with the lowest dielectric constant. VT-4 has a dielectric constant of 2.4 and is thermally stable up to 460 $^{\circ}$C, and is therefore an attractive candidate for the new interlayer dielectric.

To replace the process of depositing polymer/SiO_2 nanocomposites with a cleaner process, alternate siloxane precursors were studied as a possible replacement for the in-situ silica deposition process, which utilized either DADBS or TEOS as a precursor. A four silicon ringed siloxane with vinyl functional groups was found to have poor incorporation due to the high vapor pressure. Vinyl-T8, a cube-like silsesquioxane with functional vinyl groups was incorporated into PPXC readily. A study investigating the properties of vinyl-T8 films based on different pyrolysis temperatures revealed complex behavior, with formation of polymerized vinyl-T8 and some silica-like structure at still higher temperatures. Composites of vinyl-T8 and PPXC deposited below 5 ^{o}C exhibited precipitation of micron-sized cubic crystals of vinyl-T8. Films deposited above that temperature had n values ranging from 1.3 to 1.66, depending on the deposition conditions. Conversion of the siloxane phase into silica through post-deposition annealing was not successful, as the films degraded at 500 ^{o}C. X-ray diffraction spectra of composites contained peaks which were not characteristic of neither PPXC nor vinyl-T8, suggesting block copolymerization of a semicrystalline copolymer. Thus though a silica phase could not be achieved, the resulting composite had silimar properties, achieved with a clean process. The characterization of the composite films shed some light into the behavior of composites of organic and inorganic polymers.

Future Work

Many questions were raised throughout the completion of this work. Further investigation would lead more insights and revelations in the field of chemical vapor deposition of polymers and organic/inorganic polymer composites. A deposition kinetics study with a large number of repetitions needs to be done to substantiate the results presented here and determine the variance in the deposition rates. A more precise understanding of the gas flows within the reactor would help determine what improvements need to be made in the design to raise deposition rates and achieve greater film uniformity. The major question that rouse out of this part of the work was why there was such a large variance in the data. While variables which were not included in the study surely contributed to the variance of the data, further experiments would need to be done to arrive at any valid conclusions. The composites of organic parylene polymers and inorganic siloxane polymers turned out to be quite complicated.

This study revealed the presence of parylene polymer, vinyl-T8, polymerized vinyl-T8, as well as possibly polymerized vinyl-T8 and parylene copolymer. In addition, all three polymer species exhibit some crystallization. However, the present research did not yield any quantitative details about the relative amounts of these polymer species or the extent of the crystallization. Furthermore, the nature of the bonding between the species as well as any unpolymerized species has not been determined. The nature of these bonds is very relevant to the behavior of the film as a whole, especially with regard to the thermal stability. Any future work in this area should focus on answering this main question, namely establishing more clearly the relationship between the deposition conditions, such as the deposition temperature and the sublimation rates, and the relative quantities of the various polymer species and their amorphous and semicrystalline phases. The size of the clusters of these various polymer species as well as their distribution should also be analyzed. The pyrolysis temperature of vinyl-T8 has been shown to determine the extent of polymerization as well as formation of a silica-like phase. Since the same bonds are involved in vinyl-T8, polymerized vinyl-T8 and the silica-like phase, analytical techniques which yield results on the order of the bond length cannot

distinguish between them. Thus the long range order of the films has not been described, and neither has the type of bonding between the various phases. Since the silica-like phase is desirable, determining what deposition conditions maximize it is of importance.

More x-ray diffraction analysis needs to be done to understand the morphology of VT-4. The same is true for the PPXC/vinyl-T8 composites. Studies to determine molecular weight need to be performed. TEM images should be taken to obtain more information about the morphology. A myriad characterization techniques could be applied to gain a deeper understanding of this material system.

Lastly, the feasibility of this work being incorporated into industrial processes needs to be addressed. The semiconductor industry is very conservative and the incorporation of any new process is done very carefully and after extensive testing. Whether or not the material system studied in this work has any potential future in the industry depends on how much further study will be done. At this point, there is not enough information to conclude that polymer/siloxane composites could be used as a new low-k dielectric. The behavior of the various phases and their distribution needs to be understood first to ensure consistent film properties. The interaction of this dielectric with the other materials to be used in the fabrication of an integrated circuit is unknown. Thus, while some of the requirement for a new low-k dielectric are satisfied, without testing the material *in-situ*, in the place of the old dielectric, where potential problems might be uncovered, a recommendation cannot be made.

VITA: Viktor Simkovic

The author was born in 1975 in a small town called Malacky, in the country of Slovakia. At the age of 11, his family escaped to Austria through Yugoslavia for political reasons. After a year and a half, the whole family moved to the United States. The author started high school in New York City at the Bronx High School of Science. After moving to Virginia, he graduated from the Thomas Jefferson High School of Science and Technology.   He then went on to receive two Bachelor of Science degrees from Virginia Tech, in Materials Science and Engineering and Mathematics. He then stayed on to get his Master of Science in Materials Science and Engineering, of which the present work is the thesis.